ND ISOTOPES TRACK RARE EARTH ELEMENT SOURCES IN ACID MINE DRAINAGE, APPALACHIAN BASIN, USA

By

Irene Langtry Rizza Wallrich

B.A. Geology, SUNY Geneseo, 2008

M.S.T. Environmental Science, University of Utah, 2011

Submitted to the Graduate Faculty of the

Kenneth P. Dietrich School of Arts and Sciences in partial fulfillment

of the requirements for the degree of

Master of Science in Geology

University of Pittsburgh

2017

UNIVERSITY OF PITTSBURGH

Kenneth P. Dietrich School of Arts and Sciences

This thesis was presented

by

Irene Langtry Rizza Wallrich

It was defended on

November 10th, 2017

and approved by

Brian Stewart, Associate Professor, Department of Geology & Environmental Science

Charles Jones, Lecturer & B.S. Programs Advisor, Department of Geology & Environmental Science

Thesis Director: Rosemary Capo, Associate Professor, Department of Geology & Environmental Science

ND ISOTOPES TRACK RARE EARTH ELEMENT SOURCES IN ACID MINE DRAINAGE, APPALACHIAN BASIN, USA

Irene Langtry Rizza Wallrich, M.S.

University of Pittsburgh, 2017

Acid mine drainage (AMD) has been proposed as a potential source of strategic rare earth elements (REEs). To simulate AMD-rock interactions and determine the source of energy-critical REEs, we conducted experiments using overburden, coal (Pittsburgh Coal), and underclay samples from an AMD generating mine in the Appalachian Basin. Sulfuric acid (0.05N) leached < 10% of whole rock total REEs from all samples except the underclay, which released 35%. Unlike the relatively flat North American Shale Composite (NASC) normalized whole rock REE patterns, sulfuric acid leachates of these units show middle rare earth element (MREE) enrichment patterns similar to what is observed in AMD.

Measured $\varepsilon_{Nd}(0)$ values for the whole rocks range from -11.2 to -12.0. Most leachates for those rock units have more radiogenic $\varepsilon_{Nd}(0)$ values between -5.8 and -9.3, similar to that of AMD from the Pittsburgh Coal. When corrected to a late Carboniferous depositional age (300Ma), the $\varepsilon_{Nd}(T)$ range for all samples (whole rocks and leachates) narrows to -9.9 to -6.2 for all samples. These data, together with geochemical and petrographic analysis, suggest that the MREE enrichment of AMD results from preferential leaching of a readily dissolvable, MREE-rich, high Sm/Nd mineral phase such as carbonate or phosphate accessory minerals.

TABLE OF CONTENTS

LIST OF TABLES

LIST OF FIGURES

PREFACE

This project would not have been possible without the generous financial support of the Whittington Family and the University of Pittsburgh. I would like to acknowledge the guidance and support of Drs. Rosemary Capo and Brian Stewart as this project evolved. Thank you for teaching me the skills necessary to make this project a reality. I would also like to thank my committee member, Dr. Charles Jones, for his many insights and interesting antidotes during my time at the University of Pittsburgh.

My lab mates - Monica McGrath, Justin Mackey, Ben Hedin, Zachary Tieman, Corine Hite, and Anna Thornton -, fellow graduate students, and post-doctoral fellows in the Department of Geology and Environmental Sciences have been incredible source of support. You are amazing people. I cannot thank you enough for your friendship, collaboration, and encouragement. I would especially like the thank Dr. Thai Phan. Your guidance in the lab was invaluable, and it has been a pleasure to work with you.

A special thanks to Tracy Bank, Phillip Tinker and William Garber for their research insights. I have greatly benefited from your generosity, both with your time and your knowledge.

Most importantly, I would like to thank my extraordinary family whose love and encouragement made this possible. I owe my deepest gratitude to my parents for encouraging educational pursuits and emphasizing the value of knowledge; my siblings for always being there when I need a pep talk; and Blake Wallrich for his love and support.

1.0 INTRODUCTION

Mine drainage is a serious environmental concern due to its ability to mobilize and transport metals into streams and groundwater (Johnson and Hallberg 2005; Cravotta 2008a; Nordstrom 2011; Blowes et al. 2014). This ubiquitous waste stream from metal workings and coal mines results from the oxidation of sulfide minerals when exposed to oxygen and water. Pyrite (FeS_2), an abundant sulfide mineral common to both coal and ore deposits, is often used to illustrate acid generating sulfide oxidation reactions (Nordstrom and Alpers 1999; Johnson and Hallberg 2005; Akcil and Koldas 2006; Blowes et al. 2014; Simate and Ndlovu 2014; Nordstrom, Blowes, and Ptacek 2015):

$$FeS_2 + {}^{15}/_4\, O_2 + {}^{7}/_2\, H_2O \rightarrow Fe(OH)_3\,(s) + 2H_2SO_4 \qquad \textit{[Rxn. 1]}$$

The above reaction summarizes a two-step oxidation process where both oxygen and ferric iron act as oxidizers (over-simplification of the oxidation process):

$$FeS_2 + {}^{7}/_2\, O_2 + H_2O \rightarrow Fe^{2+} + 2SO_4^{2-} + 2H^+ \qquad \textit{[Rxn. 2]}$$

$$Fe^{2+} + {}^{1}/_4\, O_2 + {}^{7}/_2\, H_2O \rightarrow Fe(OH)_3\,(s) + 2H^+ \qquad \textit{[Rxn. 3]}$$

Each mole of pyrite oxidized generates one mole of Fe^{2+}, two moles of SO_4^{2-}, and four moles of H^+ (Blowes et al. 2014). Several chemical (Fe^{3+} reactivity, site mineralogy, pH, Eh, etc.), physical (temperatures, surface area, permeability, etc.) and biological (microbial populations) factors determine the rate of the above reactions at a given site (Nordstrom and Alpers 1999; Plumlee et al. 1999; Akcil and Koldas 2006; Nordstrom 2011; Blowes et al. 2014;

Nordstrom, Blowes, and Ptacek 2015). The acid generated dissolves carbonate, oxide, and aluminosilicate minerals, resulting in elevated concentrations of Al, Mn and heavy metals in mine drainage (Akcil and Koldas 2006; Cravotta 2008a).

Flows of acidic, metal-polluted (e.g., iron, aluminum, arsenic) waters can continue for decades after operations have ceased, degrading water quality, reducing aquatic diversity, and corroding infrastructure (Younger 1997; Johnson and Hallberg 2005; Cravotta 2008a; Jennings, Blicker, and Neuman 2008; Simate and Ndlovu 2014). Acid mine drainage (AMD) is a global problem, both for countries with under-regulated to nonregulated mining industries operating today, and for regions with historic mines that operated with little to no regulation. The Appalachian Basin is an example of the latter, with extensive coal resources and a long mining history. It is estimated that in Pennsylvania alone, over 4,500 km of waterways have been affected by AMD (USGS 2010).

In addition to metals, AMD contains elevated concentrations of rare earth elements (REEs) (Cravotta 2008a; Cravotta 2008b; Ayora et al. 2015). When normalized to a shale composite, REEs in AMD commonly show a middle rare earth element (MREE)-enriched pattern, which is characteristic of natural and anthropogenically impacted acidic waters (Worrall and Pearson 2001; Merten et al. 2005; Pérez-López et al. 2010; Stewart et al. 2017). REEs, lanthanide series elements (La-Lu), have unique chemical and physical properties that result from their trivalent charge. In addition to their similar valence state, the ionic radii of REEs systematically decrease down series (lanthanide contraction), resulting in predicable chemical behavior within this suite of elements. These properties allow for the retention of source signatures through weathering, transport, and diagenesis, making REEs powerful tracers of geochemical processes like petrogenesis and water-rock interactions in aqueous environments

(Elderfield, Upstill-Goddard, and Sholkovitz 1990; McLennan et al. 1993; Johannesson and Zhou 1999; Worrall and Pearson 2001).

The unique chemical and physical properties of the REEs, have also made them critical components of lamp phosphors, catalysts, and electronics, notably permanent magnets and rechargeable batteries (DOE 2011; Binnemans et al. 2013; Commission 2014; Gunn 2014; Ayora et al. 2015). Due to concerns with global market supply and increasing demands for REEs in growing technological sectors, the search for alternative sources of these critical elements (notably: Nd, Dy, Tb, Eu, Yb) has become a growing priority for many countries (Figure 1) (DOE 2011; Binnemans et al. 2013; Commission 2014). It should be noted that of the five elements identified as critical by the U.S. Department of Energy, MREEs (Sm-Dy) are disproportionally critical relative to light- (La-Pm) and heavy- (Ho-Lu) REEs.

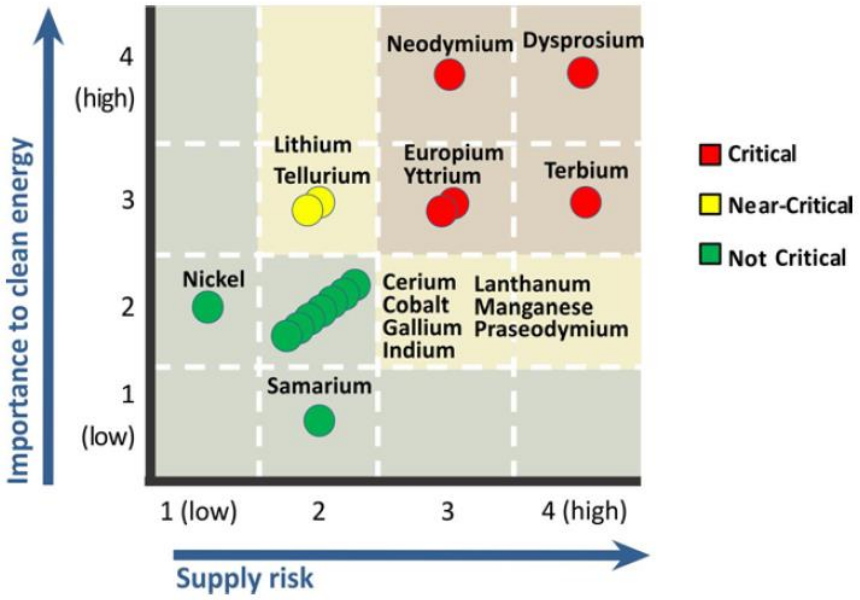

Figure 1. Clean energy technology criticality matrix (DOE 2011). The U.S. Department of Energy (DOE) evaluated 16 elements to assess their role in the clean energy economy. Five REEs, including neodymium, were found to be of high importance with potential supply challenges. For these reasons, these elements have been identified as critical from 2015 to 2025.

Recent demand for alternate sources of REEs has resulted in several studies investigating the feasibility of economic REE recovery from coal deposits and coal by-products like AMD and coal fly ash (Seredin and Dai 2012; Ayora et al. 2015; Franus, Wiatros-Motyka, and Wdowin 2015; Ziemkiewicz et al. 2016). Should mine drainage prove to be a viable source of REEs, an understanding of these complex chemical systems is imperative to assess resource potential from these nearly perpetual waste streams (Seredin and Dai 2012; Ziemkiewicz et al. 2016).

REE concentrations in natural waters are a function of solution chemistry, the concentration and reactivity of REE sources in the local substrate (soil or bedrock), and geochemical and biogeochemical processes (mixing, sorption-desorption, precipitation, colloid formation, ion exchange, redox and biological factors) (Humphris 1984; Braun and Pagel 1990; Elderfield, Upstill-Goddard, and Sholkovitz 1990; Sholkovitz 1995; Dia et al. 2000; Ingri et al. 2000; Welch et al. 2009). However, the source of MREE-enrichment found in acidic waters remains uncertain (Åström and Corin 2003; Olías et al. 2005; Zhao et al. 2007). Several studies have proposed various source- and process-driven controls for this distinctive pattern, including preferential leaching of a MREE-enriched mineral phase in local strata (Worrall and Pearson 2001; Merten and Buchel 2004; Leybourne and Cousens 2005; Merten et al. 2005; Wood, Shannon, and Baker 2005; Sun et al. 2012); MREE mobilization by S-species complexation during pyrite oxidation (Grawunder, Merten, and Buchel 2014); fractionation by colloidal complexes (Åström and Corin 2003); solid-liquid exchange reactions with surface coatings and/or clays (Gimeno Serrano, Auqué Sanz, and Nordstrom 2000; Leybourne et al. 2000; Åström 2001; Coppin et al. 2002; Gammons, Wood, and Nimick 2005); preferential removal through the formation of secondary minerals (Welch et al. 2009); and variable complex stabilities for REE (Tang and Johannesson 2003).

This study investigates the origin of REEs in northern Appalachian Basin coal mine drainage, by determining the geochemical characteristics and isotopic signatures of (1) AMD from Pittsburgh Coal discharges (2) whole rock samples from a representative stratigraphic section, and (3) the fraction of readily leachable REEs within the local strata. Constraining the origin of REEs in AMD will increase understanding of water-rock interactions and weathering in this system, and clarify the controls responsible for the MREE-enrichment observed in AMD.

In this study, neodymium (Nd) isotopes were used as unique tracers of REE provenance and mobility in AMD. Due to the similar chemical and physical properties of lanthanide series elements, the source and transport behavior of Nd (a REE) should be an ideal proxy for the behavior of the REE suite. Additionally, the Nd-Sm isotope system is a powerful tool for determining origin, as minerals have different affinities for incorporating Sm into their crystal structure at the time of formation. Over geologic time, mineral $^{143}Nd/^{144}Nd$ ratios (^{144}Nd is a stable isotope) diverge due to the radioactive decay of ^{147}Sm into ^{143}Nd (half-life = 106 b.y.). This results in minerals with unique $^{143}Nd/^{144}Nd$ ratios that are a function of the original ^{147}Sm the concentration, for example minerals with high Sm/Nd ratios will develop high $^{143}Nd/^{144}Nd$ ratios. Rock units also have unique Nd isotope compositions, resulting from the average Nd signature of all the minerals that make up the unit.

Filtration experiments were also conducted to constrain colloidal influences in this system, specifically to determine whether REEs are fully dissolved or sorbed to a solid phase. This has implications for water-rock interaction interpretations, as the partitioning of REEs between the solid and aqueous phase is a control on REE transport and behavior that is independent of source.

2.0 GEOLOGIC SETTING

The Pittsburgh Coal of the Monongahela Group was deposited in the Appalachian Basin, a laterally extensive, NNE-SSW trending, peripheral foreland basin that spans the eastern margin of North America, during the Upper Pennsylvanian Period (Castle 2001) (Figure 2). The basin formed during the Paleozoic Wilson cycle that began with the rifting of Rodina and ended with the convergence of Gondwana and Laurentia, which closed the Iapetus Ocean and formed the supercontinent Pangea (Faill 1997; Hatcher 2010). During this period, the eastern margin of Laurentia was impacted by three successive orogenies, the Taconic, the Acadian, and the Alleghenian, which resulted in thick sediment accumulations in the foreland basin (Castle 2001; Hatcher 2010). Glacio-eustatic controls on sea-level and fluctuating tectonic and climatic controls on sedimentation have been preserved in the extensive stratigraphic record within the basin, which includes the carboniferous age coals beds (Greb et al. 2008; Heckel, Gibling, and King 1998; Klein and Kupperman 1992; Cecil 1990).

Basin formation during the carboniferous period is largely attributed to tectonic loading of the Alleghenian orogeny and has been characterized as a relatively broad, shallow foreland basin (Tankard, 1986, Ettensohn, 1994). Detrital sediments from the ancestral Appalachian Mountains (source to the south) and the Canadian Shield (source from the north) formed elongate deltaic fans across a broad coastal plain adjacent to the Alleghenian fold and thrust belt (Arkle 1974; Donaldson 1974; Ruppert et al. 2002). Strata of the Monongahela Group, the

underlying Conemaugh group, and the overlying Dunkard group, represent a period of evolution from shallow-water deltas to alluvial plains and flood basins (Donaldson 1974). Much of the strata in the Upper Pennsylvanian though Lower Permian interval are terrestrial to marginal-marine siliciclastic units, with lesser amounts of limestone and coal. Peat deposits are associated with a regional, west sloping alluvial plain that graded to a shallow marine environment to the west (Arkle 1974; Edmunds, Skema, and Flint 1999).

The Monongahela Group ranges in thickness from 73 to 130 m and consists of interbedded red and grey shales and clays, lacustrine limestones, thin-bedded sandstones and siltstones, and coals (Figure 3) (Arkle 1974; Ruppert et al. 1999; Karacan 2009) deposited on fluvial dominated deltas in the coastal plain (Donaldson 1974; Cecil et al. 1985). Eustatic sea-levels changes, coupled with a hiatus in detrital supply, resulted in the development of widespread, transgressive, fresh-water swamps (peat mires) on the upper deltas (Donaldson 1974; Tewalt et al. 2001; Cecil 1990). This lead to the formation of several coal deposits, most notably the Pittsburgh Coal of the Pittsburgh Formation, which delineates the Monongahela Group from the underlying Conemaugh Group (Ruppert 2000).

The Pittsburgh Coal extends over 13,000 km^2 through OH, PA, WV and MD (Figure 4). It is the thickest and most extensively mined coal unit in the Appalachian Basin (Ruppert et al. 2002), and the third largest producing coal bed in the United States (EIA 2016). Over the last two centuries, this unit has produced more coal than any other bed in the nation (Watson et al. 2001; Ruppert et al. 2002). It is a high rank, high volatile, bituminous coal with variable ash and sulfur content (Ruppert et al. 1999; Ruppert and Rice 2000; Ruppert et al. 2002). It is estimated that, of the original total resource (30 billion tons), 14.5 billion tons of the Pittsburgh Coal

remain unmined. The largest portion of this remaining resource is in Southwestern PA (Ruppert et al. 1999; Tewalt et al. 2001; Watson et al. 2001).

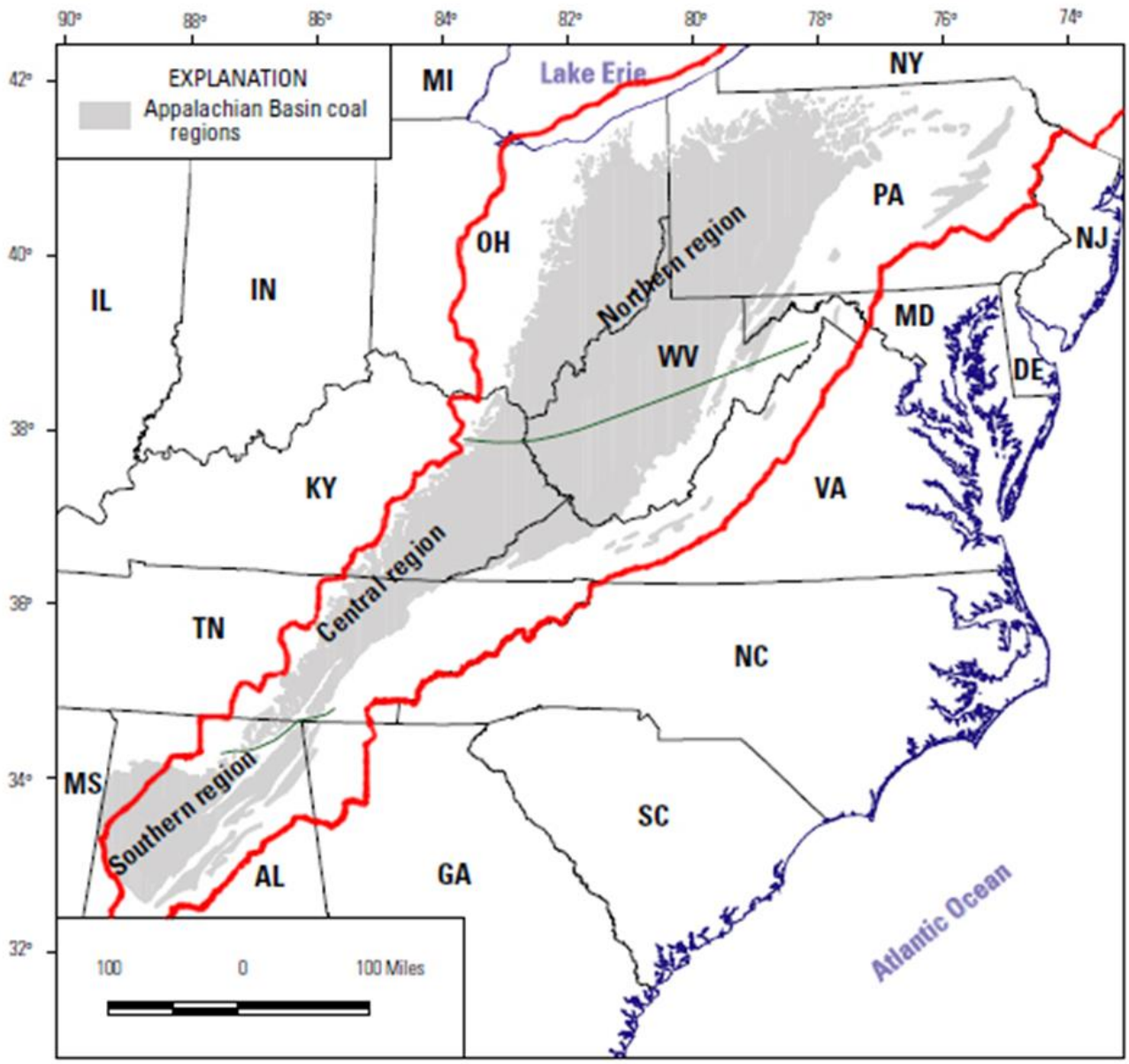

Figure 2. Map of the Appalachian Basin Province (outlined in red - as delineated by Ryder (2008)). Areas of bituminous coal are shaded in gray, and Appalachian Basin coal regions are labeled and divided by green lines (Modified from Ruppert, 2002).

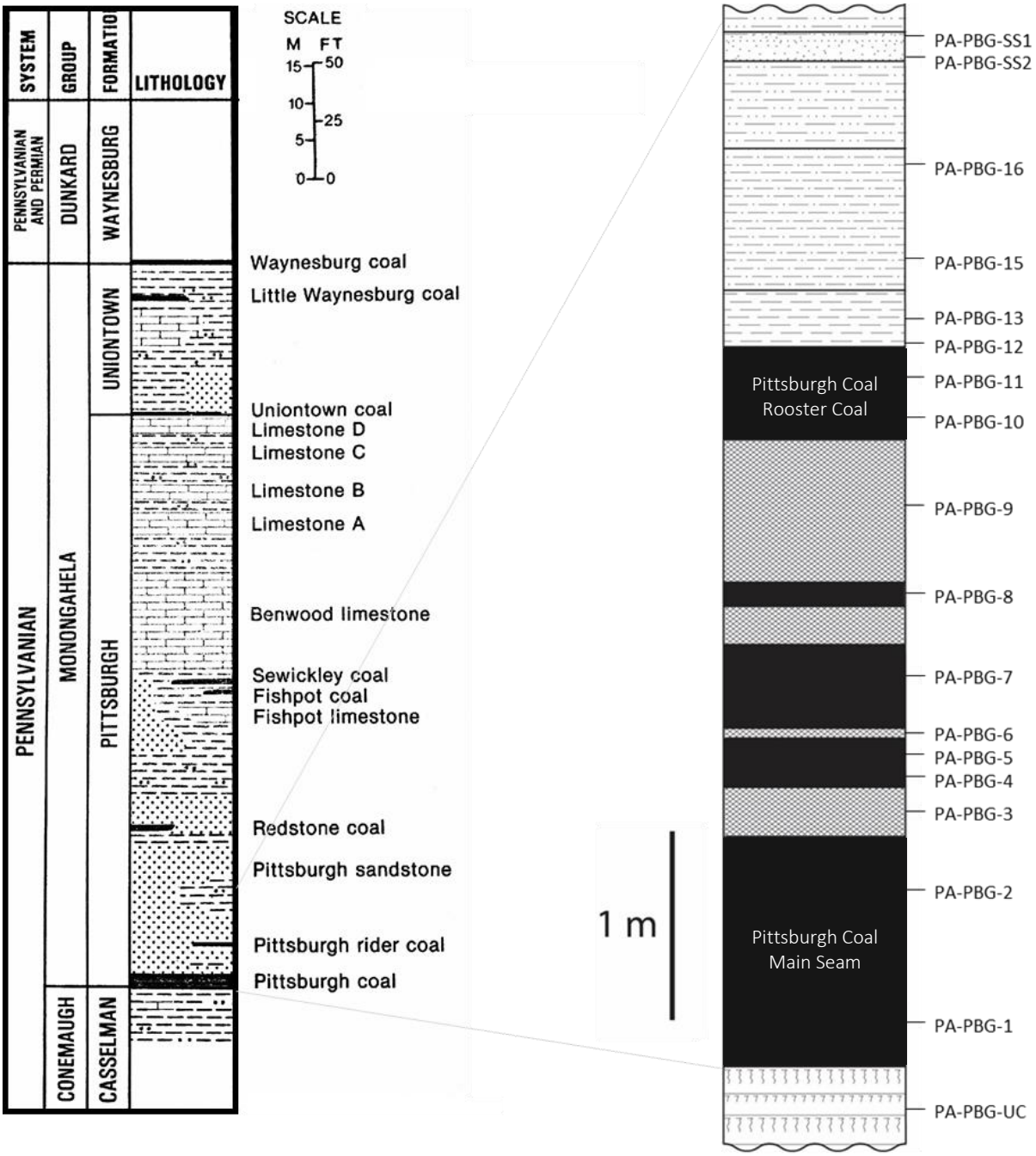

Figure 3. Generalized stratigraphic section of the Monongahela Group (from Edmunds, Skema and Flint 1999). The sampled section of the lower Pittsburgh formation is expanded, with sampling locations labeled.

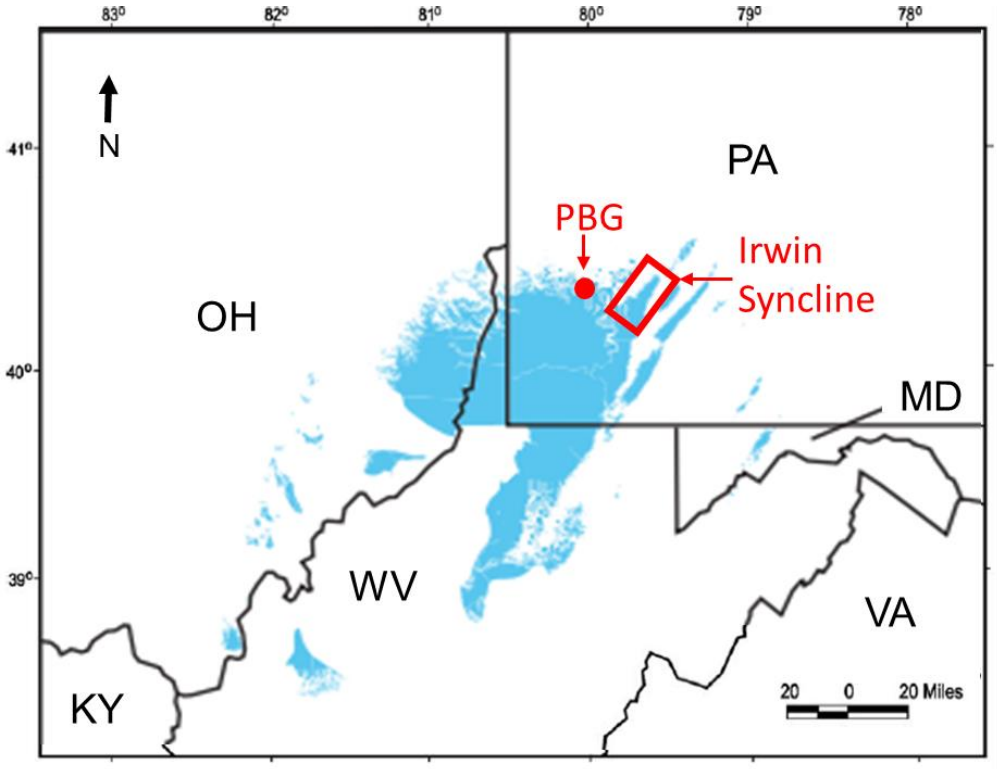

Figure 4. Map of the Pittsburgh Coal bed (shaded in blue) of the Upper Pennsylvanian, Monongahela Group (modified from Ruppert, 2002). The primary field site (PBG) is indicted in with a red dot and the Irwin syncline is outlined by a red rectangle**.**

3.0 METHODS

3.1 SAMPLE COLLECTION & PREPARATION

3.1.1 The Lower Pittsburgh Formation

The primary field site for this study is located in the Pittsburgh Botanic Gardens (PBG), approximately 14 km west of downtown Pittsburgh in Allegheny County, Pennsylvania (Figure 4). The sampling site is 400 m south of the visitor center on Pinkerton Run Road (Figure 5). In 2011, as part of an ongoing reclamation project, the PBG authorized the re-mining of an abandoned Pittsburgh Coal deep mine on the property, which was producing untreated AMD (Czebiniak 2016). Subsequent surface mining allowed for the sampling of a representative stratigraphic section of the lower Pittsburgh Formation, including the underclay, main Pittsburgh Coal seam, clay partings, roof coal, clastic overburden units, and mineral separates of pyrite from the main coal seam (Figure 6, Figure 7 and Figure 8). A flow chart detailing sample collection and analysis can be found in Figure 9.

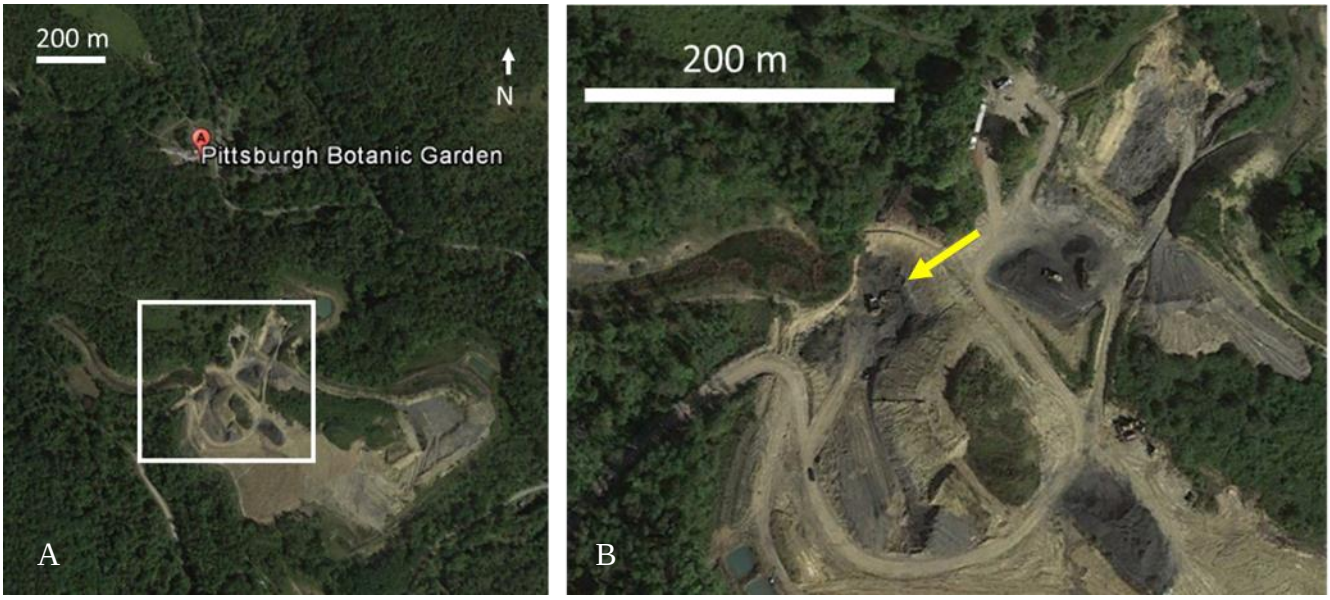

Figure 5. Satellite imagery of the PBG sampling site (images courtesy of Google, DigitalGlobe, 2016). (A) The location of the surface mine relative to the PBG visitor center (labeled Pittsburgh Botanic Garden). Sampling site is located within the white rectangle. (B) An enlarged image of the sampling site (yellow arrow indicates the sampling site).

Figure 6. PBG strip mine, March 8, 2016.

Figure 7. PBG mine sample site, March 8, 2016 (note the rock hammer on the right for scale).

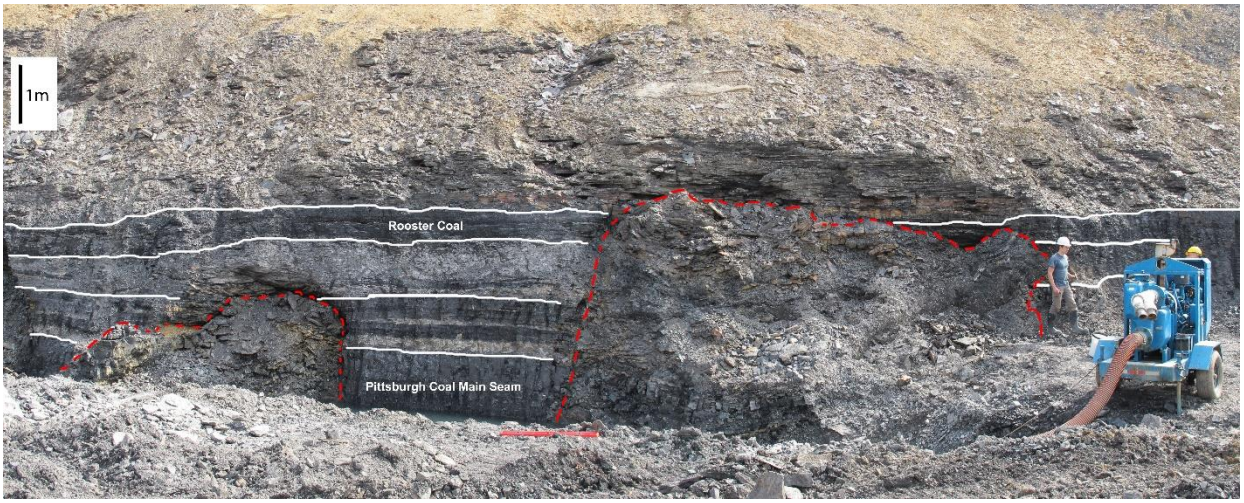

Figure 8. PBG mine stratigraphic section sampled. The columns from previous mine operations are delineated by the red dashed lines. White lines show the lateral correlation extent of major units. The main Pittsburgh Coal bed is labeled, as well as the Rooster Coal that marks the top unit of the Pittsburgh Coal.

Whole rock samples were powdered in a Ti-carbide ball mill and split for analysis. One split was reserved for major and trace element analysis. A second split (~2 g) was sequentially leached with ultrapure reagents. For sequential extraction powdered samples were leached for 4 hours with 1 N ammonium acetate buffered to a pH of 8 to remove easily exchangeable ions.

This was followed by a rinse with ultrapure (MilliQ 18MΩ) water (MQW). The residues were then leached with 0.05 N sulfuric acid (pH = 1.3) for 4 hours to mimic the effects of AMD (Rxn.1). All leaches were conducted at a 1:40 sample:liquid ratio and all leachates were filtered to 0.22 μm (Figure 9).

Pyrite nodules from the Pittsburgh Coal main seam (PBG-1) were coarsely crushed and manually separated from coal samples. Pyrite was then finely crushed and separated from organic matter using bromoform heavy liquid density separation. Bromoform was washed from pyrite using acetone and ethanol rinses, sample was dried between rinses. Dried mineral separates were split and analyzed for elemental composition (Figure 9).

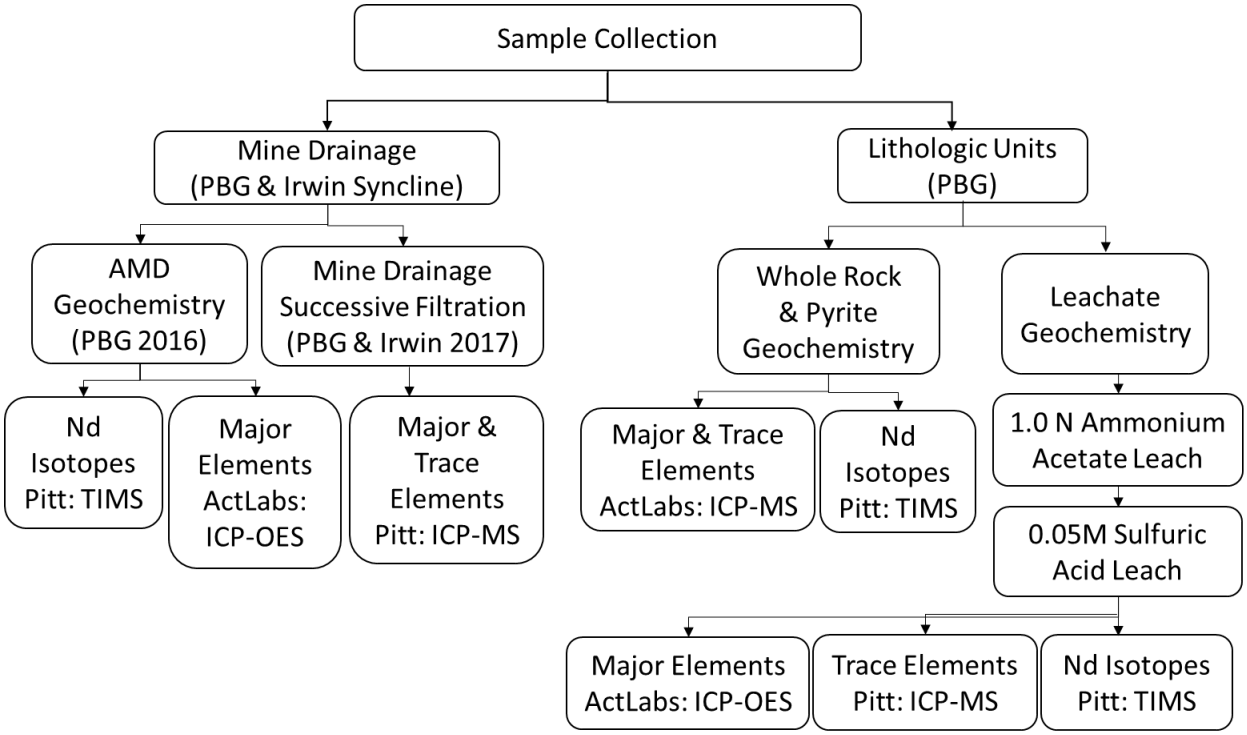

Figure 9. Method flow chart for sample preparation and analysis.

3.1.2 Acid Mine Drainage

AMD samples from an adjacent Pittsburgh Coal deep mine on the PBG property (approximately 800 m northwest of the surface mine sampling site) were collected for geochemical analysis in December 2016. Samples were collected from an underground pipe that feeds into the PBG passive treatment system installed by Hedin Environmental. Samples were filtered to 0.45 μm in acid-washed polypropylene bottles and acidified with ultrapure HNO_3 to a pH < 2.0. Field measurements of AMD included pH, temperature, conductivity, and alkalinity.

AMD was also collected from the PBG in April of 2017 for filtration experiments that investigated potential colloidal controls on REE chemistry. Three replicates of unfiltered, 0.45 μm filtrate, and 0.22 μm filtrate were collected. Three additional unfiltered samples were collected with no headspace, brought back to the lab at the University of Pittsburgh, and centrifuged through a 3 kDa molecular weight cut-off (MWCO) membrane filter within 3 hours of collection. All samples were acidified with ultrapure HNO_3 to a pH < 2.0 in acid-washed polypropylene bottles.

Filtration experiments were also conducted at four Pittsburgh Coal mine drainage sites within the Irwin Syncline, southwest of Pittsburgh, in May of 2017 (Figure 4). The Irwin syncline is a plunging, NE-SW trending syncline with multiple mine drainage discharges that range from low pH to circumneutral (Winters and Capo 2004). The collection procedure used at the PBG was repeated at the Export, Delmont, Irwin, and Lowber mine discharge sites.

All samples for the AMD filtration experiments, both filtered and unfiltered, were hot block digested using a 1:5 ratio of ultrapure concentrated HCl: HNO_3. A 25 mL aliquot of each sample was digested at 95^{o}C for a total of 90 minutes, covered for the first 45 minutes and

uncovered for the remaining 45 minutes. All samples were then brought up to a final volume of 30 mL with 2% HNO_3. It should be noted that the PBG samples collected in 2016 and analyzed for major and trace element geochemistry, were filtered and acidified in the field and did not require hot block digestion.

3.2 ANALYTICAL METHODS

3.2.1 Elemental analysis

Concentrations of major and trace elements in whole rock and pyrite samples collected from PBG in 2016 were determined by ICP-MS, at Activation Laboratories (ActLabs), Canada. In addition to elemental analysis, sulfur speciation analysis and proximate analysis (moisture, ash, volatile matter, fixed C) were conducted on coal samples at ActLabs. Ash content, the residue remaining after moisture, volatiles and fix carbon have been driven from the sample, was used as a relative estimation of mineral matter in the coal samples. Petrographic analysis was also used to determine preliminary mineralogic composition of siliciclastic samples.

Ammonium acetate leachates, sulfuric acid leachates and PBG AMD (collected in 2016), were analyzed for 36 elements (including major elements, trace metals and Si) by ICP-OES at ActLabs. Leachates were also analyzed for REEs on a Perkin-Elmer ICP-MS at the University of Pittsburgh. Major element and REE concentrations for AMD filtrates collected in 2017 were determined using a Perkin Elmer ICP-MS at the University of Pittsburgh (Figure 9).

3.2.2 Neodymium isotopes

Neodymium isotope preparation and analysis were carried out under clean laboratory conditions at the University of Pittsburgh. Powdered whole rock samples were acid digested (HNO_3, $HClO_4$, and HF) and evaporated to dryness in Teflon vials at 120^{o}C under HEPA filtered airflow. Aliquots of leachate and AMD samples were also evaporated to dryness in Teflon vials at 120^{o}C under HEPA filtered airflow. To fully dry down sulfuric acid leachates, samples were treated with H_2O_2 to the hydrophilic sample behavior that was attributed to the formation of organosulfides. All samples were then re-dissolved in 1.5N HCl.

REEs were then separated from the sample matrix using cation exchange columns eluted with dilute HCl. Nd was separated from other REEs using LnSpec® resin packed columns, eluted with dilute HCl. An aliquot containing approximately 150 ng of Nd was the evaporated under HEPA airflow conditions onto a Re filament. Nd isotopes of the sample, as well as the La Jolla Nd Standard, were measured using a Finnigan MAT 262 multi-collector thermal ionization mass spectrometer (TIMS) at the University of Pittsburgh. A total of 100 ratios were measured during each analysis.

4.0 RESULTS

4.1 GEOCHEMISTRY & REE PATTERNS

4.1.1 AMD samples

Major metal (Al, Fe, Mn, Mg, Ca, Na, K, Si), trace metal (Ag, As, Cd, Co, Cr, Cu, Ni, Pb, Zn), S and P concentrations in the PBG AMD collected in the spring of 2016 are reported in Table 1. Major (Al, Fe, Mn, Mg, Ca, Na, K) and trace (Ag, As, Cd, Co, Cr, Cu, Ni, Pb, Zn) metal data for unfiltered and filtered Pittsburgh Coal mine drainage collected in the spring of 2017 are reported in Table 2. Sulfur data (Table 1) was used in mass balance calculations that assessed pyrite as a potential source REE enrichment in AMD. Also of note are the similar trends in Al concentration (Table 2) and total REE (TREE) concentration (Table 3 and 4) in mine drainage samples relative to the pH. Both Al and TREE concentrations are inversely related to pH, and both sharply decrease in at pH > 5.

Pittsburgh Coal mine discharges with pH < 5.1 (PBG, Export, and Delmont) had TREE concentrations that ranged from 68 μg/L to 185 μg/L (Tables 3 and 4). REE concentrations in circumneutral (pH > 5.1) discharges at Lowber (pH = 6.4) and Irwin (pH = 5.9) were below the method detection limit (MDL). REE concentrations in Pittsburgh Coal AMD normalized to the North American Shale Composite (NASC) (Gromet et al., 1984) exhibited a characteristic

MREE-enriched pattern (Figure 10) similar to other AMD studies (Verplanck, Nordstrom, and Taylor 1999; Worrall and Pearson 2001; Gammons et al. 2003; Merten et al. 2005; Zhao et al. 2007; Pérez-López et al. 2010; Sun et al. 2012). REE concentrations in filtrate samples overlapped within the measurement error regardless of filter size at each AMD site, with all size fractions exhibiting the same MREE-enrichment pattern (Figure 10).

Table 1. Major element and metal concentrations (mg/L) in PBG acid mine drainage in western, PA. Samples measured by ICP-OES at Activation Laboratories.

Sample	Si	Al	Fe	Mn	Mg	Ca	Na	K	P	S	Ag	As	Cd	Co	Cr	Cu	Ni	Pb	Zn
										mg/L									
PBG-AMD-R1	15.8	19.3	0.580	1.04	45.8	86.9	10.5	1.10	< 0.02	150	< 0.005	< 0.03	<0.002	0.069	< 0.02	0.024	0.174	< 0.01	0.229
PBG-AMD-R2	15.4	18.4	0.420	0.70	47.5	104	12.4	1.00	< 0.02	192	< 0.005	< 0.03	<0.002	0.057	< 0.02	0.015	0.146	< 0.01	0.171

Table 2. Major metal (reported in mg/L) and trace metal (reported in µg/L) concentrations in filtered and unfiltered mine drainage samples from successive filtration experiments at the Pittsburgh Botanic Garden and Irwin Basin. Samples were measured by ICP-MS at the University of Pittsburgh. Note the change in units.

Sample Id	Al	Fe	Mg	Mn	Ca	Na	K	Ag	As	Cd	Co	Cr	Cu	Ni	Pb	Zn
				(mg/L)				----------	----------	----------	----------	(ug/L)	----------	----------	----------	----------
PBG Pittsburgh, PA pH=3.2																
Replicate Samples																
PBG-AMD-Raw (1)	26.1	0.696	57.4	0.138	14.7	11.5	5.25	< 3.0	< 1.2	1.80	90.2	6.28	29.5	220	0.433	274
PBG-AMD-0.45 µm (1)	26.0	0.803	57.9	0.148	15.3	12.1	5.18	< 3.0	< 1.2	1.74	94.8	6.12	32.0	236	0.399	286
PBG-AMD-0.22 µm (1)	26.6	0.745	58.2	0.148	15.0	12.1	4.92	< 3.0	1.43	2.18	93.3	6.12	30.8	230	0.424	277
PBG-AMD-3kD (1)	25.3	0.725	57.4	0.150	14.1	11.9	5.52	< 3.0	< 1.2	1.73	97.0	6.06	31.1	233	0.457	283
PBG-AMD-Raw (2)	26.0	0.718	57.6	0.140	12.3	12.0	4.94	< 3.0	< 1.2	1.94	92.7	6.15	31.1	227	0.415	274
PBG-AMD-0.45 µm (2)	25.3	0.649	55.9	0.135	13.2	11.6	4.46	< 2.9	2.06	1.69	88.0	5.30	29.2	216	0.402	275
PBG-AMD-0.22 µm (2)	25.9	0.736	56.3	0.140	15.8	11.7	4.76	< 3.0	< 1.2	1.53	91.9	6.07	29.9	223	0.400	270
PBG-AMD-3kD (2)	24.9	0.694	57.0	0.136	13.8	11.9	4.72	< 3.0	< 1.2	1.50	88.3	5.65	29.1	214	0.389	264
PBG-AMD-Raw (3)	25.9	0.670	58.2	0.136	16.2	11.6	6.70	< 3.0	1.77	1.65	90.4	5.48	30.2	225	0.377	277
PBG-AMD-0.45 µm (3)	26.4	0.683	57.8	0.131	13.2	11.5	8.34	< 3.0	1.19	2.48	84.0	5.57	28.6	209	0.416	272
PBG-AMD-0.22 µm (3)	24.9	0.640	55.9	0.135	13.2	11.1	12.6	< 3.0	< 1.2	3.07	86.9	4.96	28.8	214	0.460	290
PBG-AMD-3kD (3)	24.7	0.623	55.7	0.121	17.2	11.3	10.4	< 3.0	1.63	1.72	78.9	5.06	25.1	190	0.406	271
Sample Average																
PBG-AMD-R (AVG)	26.0	0.695	57.7	0.138	14.4	11.7	5.63	< 3.0	1.77	1.80	91.1	5.97	30.3	224	0.408	275
PBG-AMD-0.45 (AVG)	25.9	0.712	57.2	0.138	13.9	11.7	5.99	< 3.0	1.63	1.97	88.9	5.66	29.9	220	0.406	278
PBG-AMD-0.2 (AVG)	25.8	0.707	56.8	0.141	14.7	11.6	7.41	< 3.0	1.43	2.26	90.7	5.72	29.9	222	0.428	279
PBG-AMD-U (AVG)	25.0	0.681	56.7	0.135	15.0	11.7	6.87	< 3.0	1.63	1.65	88.1	5.59	28.5	213	0.418	272
Export, PA pH=3.3																
EX-AMD-R	13.6	2.45	34.4	0.161	11.1	24.4	8.11	< 3.0	< 1.2	< 1.2	37.0	2.46	9.24	97.9	< 0.34	150
EX-AMD-0.45	14.7	2.32	35.5	0.147	12.6	24.1	8.68	< 3.0	< 1.2	< 1.2	33.6	2.53	8.05	90.1	< 0.34	146
EX-AMD-0.2	14.4	2.31	36.1	0.151	12.6	24.4	10.8	< 3.0	< 1.2	< 1.2	33.5	2.38	8.14	91.4	< 0.34	167
EX-AMD-U	13.8	2.25	34.6	0.146	12.9	25.3	15.1	< 3.0	1.50	< 1.2	34.7	1.79	8.01	89.6	< 0.34	156
Delmont, PA pH = 5.1																
DEL-AMD-R	0.818	30.1	30.3	0.180	12.1	32.9	13.1	< 3.0	4.44	< 1.2	6.73	< 0.32	< 1.4	23.1	< 0.34	35.0
DEL-AMD-0.45	0.843	29.9	30.3	0.182	12.5	34.8	15.5	< 3.0	4.04	< 1.2	6.84	< 0.32	< 1.4	23.0	< 0.34	43.9
DEL-AMD-0.2	0.866	31.3	31.0	0.184	9.88	34.8	18.4	< 3.0	4.16	< 1.2	7.28	< 0.31	< 1.4	22.7	< 0.34	50.3
DEL-AMD-U	0.231	30.2	30.0	0.189	11.0	31.6	16.6	< 3.0	6.47	< 1.2	7.01	< 0.32	< 1.4	23.0	< 0.34	44.4
Irwin, PA pH= 5.9																
IR-AMD-R	< 0.078	51.7	37.3	0.139	18.7	166	17.8	< 3.0	7.21	< 1.2	2.29	< 0.31	< 1.4	5.45	< 0.34	< 13
IR-AMD-0.45	< 0.078	51.9	37.6	0.133	17.5	167	20.2	< 3.0	11.1	< 1.2	1.97	< 0.31	< 1.4	3.78	< 0.34	29.9
IR-AMD-0.2	< 0.078	51.5	37.6	0.136	15.2	166	21.8	< 3.0	9.37	1.61	2.08	< 0.31	< 1.4	4.76	< 0.34	53.1
IR-AMD-U	< 0.079	30.9	36.8	0.136	17.8	169	22.7	< 3.0	7.19	< 1.2	2.10	< 0.32	< 1.4	5.91	< 0.34	< 14
Lowber, PA pH= 6.4																
LOW-AMD-R	< 0.078	47.8	41.9	0.081	20.2	413	21.2	< 2.9	2.77	< 1.2	1.15	0.31	< 1.4	2.66	< 0.34	< 13
LOW-AMD-0.45	< 0.079	47.3	43.0	0.082	14.2	444	20.0	< 3.0	3.52	1.63	1.10	0.86	< 1.4	3.00	< 0.34	< 14
LOW-AMD-0.2	< 0.076	46.1	40.6	0.083	19.6	429	20.2	< 2.9	4.65	< 1.2	1.12	< 0.31	< 1.4	2.62	< 0.33	< 13
LOW-AMD-U	< 0.078	8.46	39.7	0.069	22.2	419	21.9	< 3.0	1.99	1.96	0.828	< 0.31	< 1.4	1.77	< 0.34	< 13

Table 3. REE concentrations (µg/L) in mine drainage filtrates from successive filtration experiments at the Pittsburgh Botanic Garden, Pittsburgh, PA. Samples were measured by ICP-MS at the University of Pittsburgh.

Location/Sample	La	Ce	Pr	Nd	Sm	Eu	Gd	Tb	Dy	Ho	Er	Tm	Yb	Lu	TREE
								ug/L							
PBG Pittsburgh, PA pH=3.2															
Replicate Samples															
PBG-AMD-Raw (1)	17.1	59.7	9.50	43.4	11.9	2.76	13.6	1.84	9.25	1.50	3.87	< 0.76	2.55	< 0.37	**178**
PBG-AMD-0.45 µm (1)	17.5	61.2	9.72	44.2	12.8	2.95	14.3	1.82	9.73	1.62	3.78	< 0.77	2.81	< 0.38	**183**
PBG-AMD-0.22 µm (1)	17.2	62.5	9.65	45.5	12.4	2.93	13.6	1.89	9.49	1.56	3.70	< 0.77	2.69	0.40	**184**
PBG-AMD-3kD (1)	17.3	62.3	10.1	45.8	12.6	2.90	13.7	1.87	9.60	1.64	3.58	< 0.76	2.64	0.38	**185**
PBG-AMD-Raw (2)	17.1	59.2	9.79	42.8	11.9	2.75	13.5	1.77	9.34	1.54	3.68	< 0.77	2.58	< 0.37	**177**
PBG-AMD-0.45 µm (2)	16.5	57.3	9.17	42.3	10.8	2.56	12.6	1.72	8.68	1.51	3.53	< 0.75	2.35	< 0.37	**170**
PBG-AMD-0.22 µm (2)	16.8	58.8	9.50	42.9	12.4	2.80	13.7	1.73	9.06	1.53	3.64	< 0.76	2.44	< 0.37	**176**
PBG-AMD-3kD (2)	16.1	57.1	9.41	41.3	11.6	2.81	13.1	1.78	8.88	1.47	3.49	< 0.76	2.55	< 0.37	**170**
PBG-AMD-Raw (3)	17.3	59.1	9.57	45.3	12.4	2.78	13.7	1.92	9.00	1.68	3.68	< 0.77	2.60	< 0.38	**179**
PBG-AMD-0.45 µm (3)	17.7	63.5	10.1	45.3	12.0	2.95	14.3	1.77	9.45	1.70	4.01	< 0.77	2.72	0.43	**186**
PBG-AMD-0.22 µm (3)	18.7	66.2	10.3	48.3	14.1	3.10	14.7	2.02	9.99	1.69	4.03	< 0.77	2.70	0.42	**196**
PBG-AMD-3kD (3)	17.2	59.1	9.22	42.9	12.5	2.95	13.3	1.78	9.49	1.54	3.55	< 0.77	2.43	< 0.38	**176**
Sample Average															
PBG-AMD-Raw	17.2	59.3	9.62	43.9	12.1	2.76	13.6	1.84	9.20	1.57	3.74	< 0.77	2.57	< 0.37	**178**
PBG-AMD-0.45 µm	17.2	60.7	9.65	44.0	11.9	2.82	13.8	1.77	9.29	1.61	3.77	< 0.76	2.63	< 0.40	**180**
PBG-AMD-0.2 µm	17.6	62.5	9.81	45.6	13.0	2.94	14.0	1.88	9.52	1.59	3.79	< 0.77	2.61	< 0.40	**185**
PBG-AMD-3kD	16.9	59.5	9.58	43.3	12.2	2.89	13.4	1.81	9.32	1.55	3.54	< 0.76	2.54	< 0.38	**177**

Table 4. REE concentrations (μg/L) in Pittsburgh Coal mine drainage filtrates from Irwin Basin successive filtration experiments. Samples were measured by ICP-MS at the University of Pittsburgh.

Location/Sample	La	Ce	Pr	Nd	Sm	Eu	Gd	Tb	Dy	Ho	Er	Tm	Yb	Lu	TREE
								ug/L							
Export, PA pH=3.3															
EX-AMD-Raw	6.19	22.1	3.48	15.6	3.94	1.11	5.68	0.80	4.36	0.77	1.76	< 0.76	1.38	< 0.37	**67.5**
EX-AMD-0.45 μm	6.70	22.3	3.57	15.6	4.14	1.01	5.73	0.81	4.14	0.76	1.83	< 0.77	1.45	< 0.38	**68.4**
EX-AMD-0.22 μm	6.22	22.3	3.59	15.0	5.47	1.09	5.59	0.79	4.64	0.72	1.55	< 0.77	1.37	< 0.37	**68.6**
EX-AMD-3kD	6.40	23.5	3.76	16.3	5.37	0.98	5.77	0.81	4.53	0.87	1.87	< 0.76	1.50	< 0.37	**72.0**
Delmont, PA pH = 5.1															
DEL-AMD-Raw	< 1.1	3.08	0.57	2.65	1.21	< 0.81	1.24	< 0.50	0.99	< 0.27	< 0.53	< 0.77	< 0.80	< 0.38	
DEL-AMD-0.45 μm	< 1.1	3.04	0.51	2.59	0.84	< 0.80	1.34	< 0.50	1.08	< 0.27	< 0.53	< 0.77	< 0.80	< 0.38	
DEL-AMD-0.22 μm	< 1.0	3.29	0.57	2.81	0.93	< 0.79	1.44	< 0.49	1.17	< 0.27	0.60	< 0.76	< 0.79	< 0.37	
DEL-AMD-3kD	< 1.1	3.31	0.56	2.95	< 0.78	< 0.80	1.29	< 0.50	1.05	< 0.27	< 0.53	< 0.77	< 0.80	< 0.38	
Irwin, PA pH= 5.9															
IR-AMD-Raw	< 1.0	0.42	< 0.29	< 0.51	< 0.77	< 0.79	< 1.1	< 0.49	< 0.49	< 0.26	< 0.52	< 0.75	< 0.78	< 0.37	
IR-AMD-0.45 μm	< 1.0	0.35	< 0.29	0.8	< 0.77	< 0.80	< 1.1	< 0.50	< 0.50	< 0.27	< 0.53	< 0.76	< 0.79	< 0.37	
IR-AMD-0.22 μm	< 1.0	0.46	< 0.29	0.6	< 0.77	< 0.80	< 1.1	< 0.50	< 0.50	< 0.27	< 0.53	< 0.76	< 0.79	< 0.37	
IR-AMD-3kD	< 1.1	< 0.27	< 0.29	< 0.52	< 0.78	< 0.80	< 1.1	< 0.50	< 0.50	< 0.27	< 0.53	< 0.77	< 0.80	< 0.38	
Lowber, PA pH= 6.4															
LOW-AMD-Raw	< 1.0	< 0.26	< 0.29	0.5	< 0.76	< 0.79	< 1.1	< 0.49	< 0.49	< 0.26	< 0.52	< 0.75	< 0.78	< 0.37	
LOW-AMD-0.45 μm	< 1.1	< 0.27	< 0.29	< 0.52	< 0.78	< 0.81	< 1.1	< 0.50	< 0.51	< 0.27	< 0.53	< 0.77	< 0.80	< 0.38	
LOW-AMD-0.22 μm	< 1.0	< 0.26	< 0.28	< 0.50	< 0.75	< 0.77	< 1.1	< 0.48	< 0.48	< 0.26	< 0.51	< 0.74	< 0.77	< 0.36	
LOW-AMD-3kD	< 1.0	< 0.26	< 0.29	< 0.51	< 0.77	< 0.80	< 1.1	< 0.50	< 0.51	< 0.27	< 0.53	< 0.76	< 0.79	< 0.37	

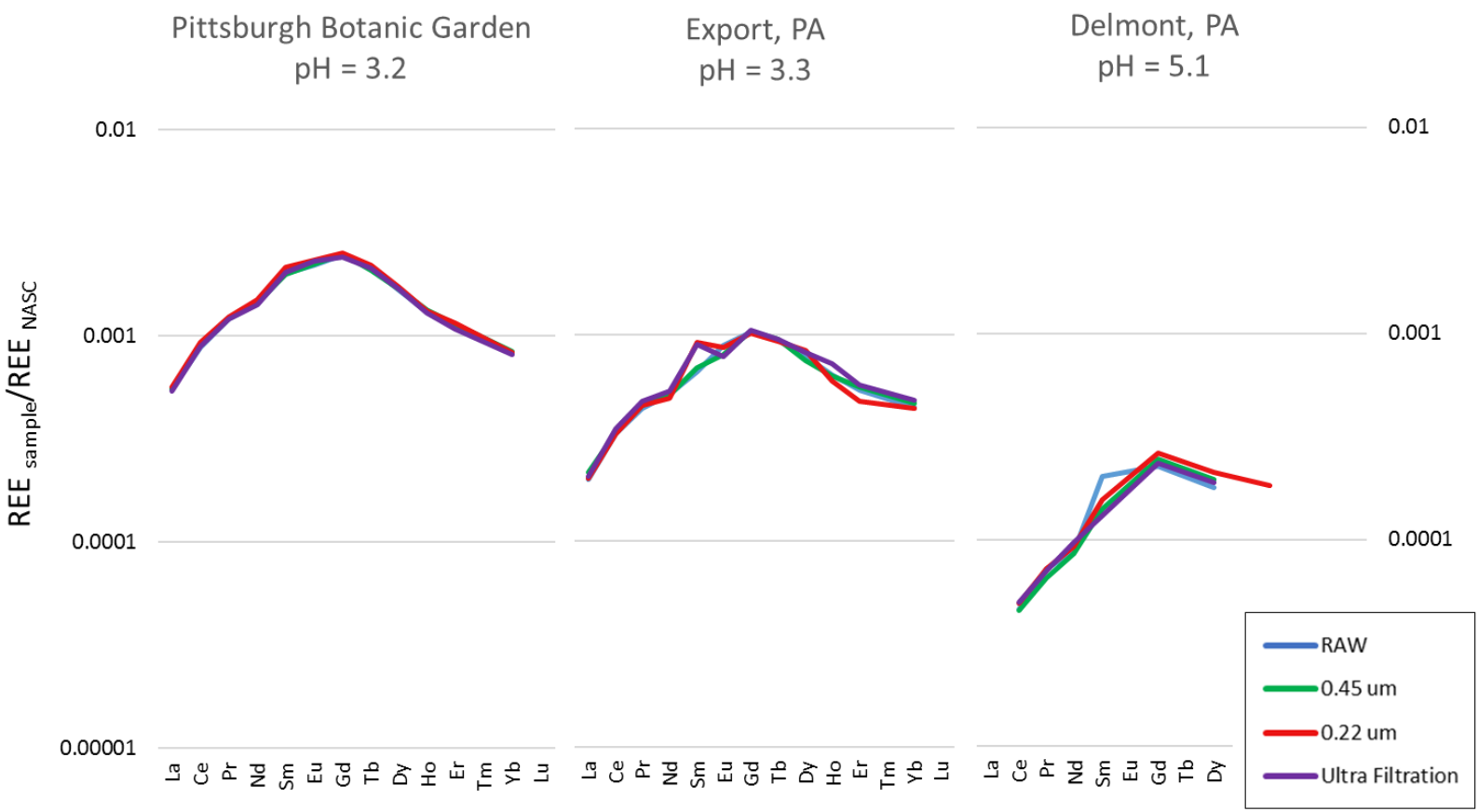

Figure 10. NASC-normalized REE patterns of unfiltered and filtered (0.45µm, 0.22µm, ultrafiltration = 3kD MWCO) Pittsburgh Coal AMD in Western, PA.

4.1.2 Whole rock & pyrite samples

Full geochemical data for all whole rock samples and pyrite are reported in Table 5 (major oxides), Table 6 (trace elements), and Table 7 (REEs). Whole rock samples included overburden sandstones and shales (TREE: 147- 296 ppm), clay partings within the coal seam (TREE: 216-256 ppm), the underclay (TREE: 377 ppm) and two coal units (Table 7). Mineralogy of the siliciclastic units is dominated by quartz, mica, and aluminosilicate clay minerals (Figure 11). Petrographic analysis suggests the possible presence of fine-grained apatite in select overburden units, as well as other accessory minerals (notably zircon) and bioclastic fragments. Pittsburgh Coal samples include the main seam (2.6% ash and TREE = 12 ppm) and a sample from higher in the section with more mineral matter (49.7% ash and TREE = 156 ppm).

As was expected, NASC-normalized REE patterns for whole rock samples from the PBG plot in a relatively flat pattern for all units, except for the main seam coal. The main seam was depleted in all REEs relative to NASC by an order of magnitude, and exhibited a greater depletion in heavy-REEs (HREEs) relatively to the other lanthanide series elements (Figure 12). Both sandstone samples had REE concentrations similar to the NASC values, whereas the clay partings, shale samples from overburden, and the underclay showed some enrichment relative to NASC for all REEs.

The TREE concentration in pyrite (~2 ppm) is two orders of magnitude below all other samples in the section, except for the main coal seam. Pyrite also shows a relatively flat, to slightly light-REE (LREE) enriched, REE pattern with a positive Eu anomaly (Figure 12). The TREE concentration for pyrite at this site is at the extreme low end of values cited for REE content in pyrite (1.5 - 66.3 ppm) by Grawunder, Merten, and Buchel (2014).

Table 5. Major element oxide concentrations (%) in whole rock samples from the PBG stratigraphic section, measured ICP-MS at ActLabs, Canada

Sample	Description	SiO_2	Al_2O_3	Fe_2O_3(T)	MnO	MgO	CaO	Na_2O	K_2O	TiO_2	P_2O_5	LOI	% Ash	Total
		%												
PBG-SS2	Sandstone	67.0	11.6	9.12	0.168	1.110	0.490	0.500	1.35	0.718	0.17	8.10		**100**
PBG-SS1	Sandstone	82.5	7.89	2.17	0.038	0.400	1.17	0.560	0.850	0.779	0.10	3.06		**99.5**
PBG-16	Shale	57.8	15.8	9.74	0.180	1.44	0.580	0.170	2.50	0.987	0.26	11.1		**101**
PBG-15	Shale	43.6	18.0	18.0	0.347	1.60	0.680	0.210	2.95	0.722	0.24	14.4		**101**
PBG-13	Shale above coal	48.1	23.0	5.74	0.085	1.30	0.390	0.230	3.02	0.791	0.20	16.8		**99.7**
PBG-9	Clay Parting	50.6	22.1	2.26	0.010	0.700	0.160	0.200	2.23	1.21	0.18	20.3		**99.9**
PBG-6	Clay Parting	57.1	25.8	1.26	0.005	0.450	0.080	0.230	2.08	1.35	0.08	12.2		**101**
PBG-4	Coal	31.1	12.7	1.74	0.004	0.430	0.060	0.120	1.60	0.622	0.04		49.7	**98.1**
PBG-3	Clay Parting	59.4	25.4	1.46	0.005	0.430	0.080	0.220	2.24	1.28	0.06	9.84		**100**
PBG-1	Main Coal Seam	1.48	0.630	0.43	0.001	0.060	0.130	< 0.01	0.010	0.03	< 0.01		2.61	**2.78**
PBG-UC	Underclay	54.0	19.8	4.70	0.024	1.30	3.47	0.230	3.26	1.01	2.20	10.3		**100**
PBG-PY1	Pyrite Nodule	0.760	0.320	60.4	0.019	0.010	0.200	0.060	0.020	0.005	< 0.01	38.9		**99.2**

Table 6. Trace element concentrations (ppm) in whole rock samples from the PBG stratigraphic section, measured by ICP-MS at ActLabs, Canada.

Sample	Ag	As	Ba	Be	Co	Cr	Cs	Cu	Ga	Ge	Hf	Mo	Nb	Ni	Pb	Rb	Sb	Sc	Sn	Sr	Ta	Tl	Th	U	V	W	Y	Zn	Zr
	ppm																												
PBG-SS2	2	< 5	253	2	15	60	1.3	10	15	1	4.8	< 2	9	< 20	14	48	< 0.5	11	2	63	1.2	0.1	7.6	2.3	62	44	24	70	202
PBG-SS1	1.4	7	158	< 1	12	230	0.9	< 10	9	2	16	3	11	20	12	31	1.6	5	2	63	1.1	0.2	10.8	2	42	34	32	30	693
PBG-16	3.5	< 5	472	3	21	90	3.8	20	20	2	7.3	< 2	15	30	17	99	< 0.5	17	3	121	1.4	0.4	13.1	3.9	107	11	43	130	301
PBG-15	2.5	< 5	515	4	16	100	6.2	30	24	2	3	< 2	13	40	18	124	< 0.5	21	3	143	1.1	0.6	12.1	3.4	142	2	42	110	107
PBG-13	< 0.5	26	526	4	30	110	9.2	70	29	2	3.7	2	14	80	45	138	2.0	19	4	214	1.2	0.9	18.3	3.8	150	6	36	130	135
PBG-9	< 0.5	16	405	3	35	120	10.4	70	29	3	5.6	3	21	60	47	124	2.1	23	7	145	1.8	0.9	18.1	4	146	8	32	60	209
PBG-6	4.4	< 5	405	2	11	100	8.5	60	25	2	5.3	< 2	21	< 20	29	110	0.7	16	4	93	2.1	0.6	17.9	4.8	92	6	33	40	204
PBG-4	-	22.9	246	2	3	120	6.7	64	18	1	3.1	< 2	9	38	32	98	1.3	24	3	67	1.0	0.7	11.1	2.6	81	-	22	41	121
PBG-3	5.1	< 5	468	3	35	120	7.1	40	32	1	5.9	< 2	22	50	40	109	0.7	16	5	133	2.1	0.7	17.2	4.4	118	6	32	110	212
PBG-1	-	142	11	< 1	1	145	< 0.5	203	1	< 1	< 0.2	< 2	< 1	154	125	< 2	2.3	27	< 1	30	< 0.1	< 0.1	0.6	0.2	5	-	2	149	6
PBG-UC	7	9	544	4	30	130	9.1	90	28	1	3.5	< 2	18	70	18	157	1.4	21	3	645	1.6	1.1	15.3	6.1	128	3	63	140	130
PBG-PY1	< 0.5	624	< 2	< 1	2	< 20	< 0.5	40	< 1	< 1	< 0.2	21	< 1	< 20	7.0	< 2	1.0	< 1	2	< 2	< 0.1	0.1	< 0.1	< 0.1	< 5	4	< 1	< 30	5

Table 7. REE concentrations (ppm) in whole rock samples from the PBG stratigraphic section, Pittsburgh, PA. Samples measured by ICP-MS at Activation Laboratories, Canada.

Sample	Description	La	Ce	Pr	Nd	Sm	Eu	Gd	Tb	Dy	Ho	Er	Tm	Yb	Lu	TREE
									ppm							
PBG-SS2	Sandstone	28.9	59.7	7.1	27.1	5.4	1.1	4.9	0.8	4.7	0.9	2.6	0.4	2.6	0.4	**147**
PBG-SS1	Sandstone	35.3	75.8	8.8	34.0	6.7	1.1	5.8	0.9	5.4	1.1	3.2	0.5	3.2	0.5	**182**
PBG-16	Shale	51.8	111	13.0	49.3	10.6	2.1	9.5	1.5	8.5	1.6	4.5	0.6	4.2	0.7	**269**
PBG-15	Shale	46.1	99.3	11.4	44.5	9.3	2.0	9.2	1.5	8.3	1.6	4.3	0.6	4.0	0.6	**243**
PBG-13	Shale above coal	58.4	124	14.3	56.6	11.6	2.2	9.6	1.4	7.4	1.4	4.0	0.6	4.0	0.6	**296**
PBG-9	Clay Parting	53.2	109	12.1	46.9	8.8	1.7	6.6	1.1	6.5	1.2	3.6	0.6	3.8	0.6	**256**
PBG-6	Clay Parting	54.9	111	11.9	42.5	7.5	1.5	5.8	0.9	5.7	1.1	3.4	0.5	3.6	0.6	**251**
PBG-4	Coal	33.2	67.9	7.7	27.0	4.9	1.0	3.7	0.6	3.8	0.8	2.3	0.3	2.1	0.4	**156**
PBG-3	Clay Parting	49.0	92.0	9.8	34.8	6.7	1.4	5.6	1.0	6.1	1.2	3.5	0.5	3.6	0.6	**216**
PBG-1	Main Coal Seam	3.0	5.6	0.6	2.2	0.4	0.1	0.4	< 0.1	0.3	< 0.1	0.2	< 0.05	0.1	< 0.01	**13.0**
PBG-UC	Underclay	78.1	158	17.8	67.3	13.7	2.9	12.4	1.9	11.4	2.1	5.6	0.7	4.3	0.7	**377**
PBG-PY1	Pyrite Nodule	0.5	0.8	0.1	0.4	0.1	0.0	0.1	< 0.01	0.1	0.0	0.0	< 0.005	0.0	0.0	**2.0**

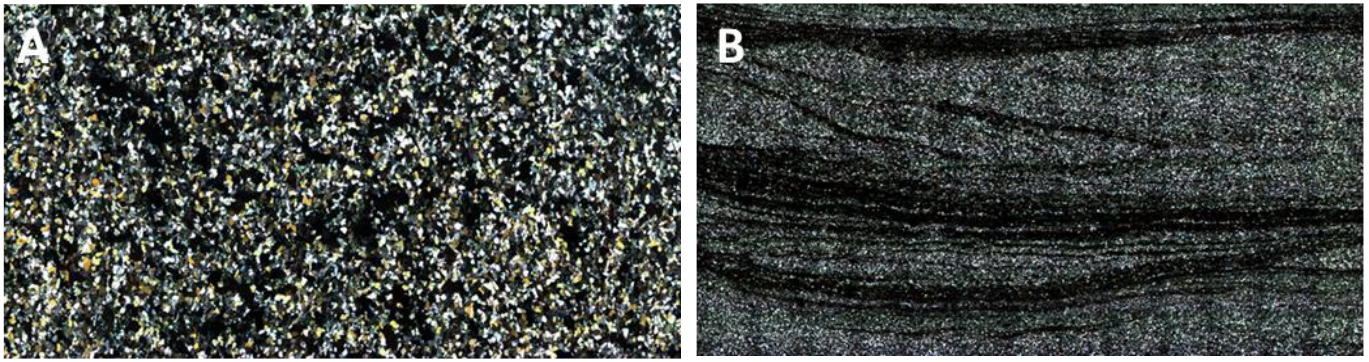

Figure 11. Photomicrographs of Pittsburgh Coal overburden sandstone (A) and shale (B) (Field of view: 33 mm x 17 mm).

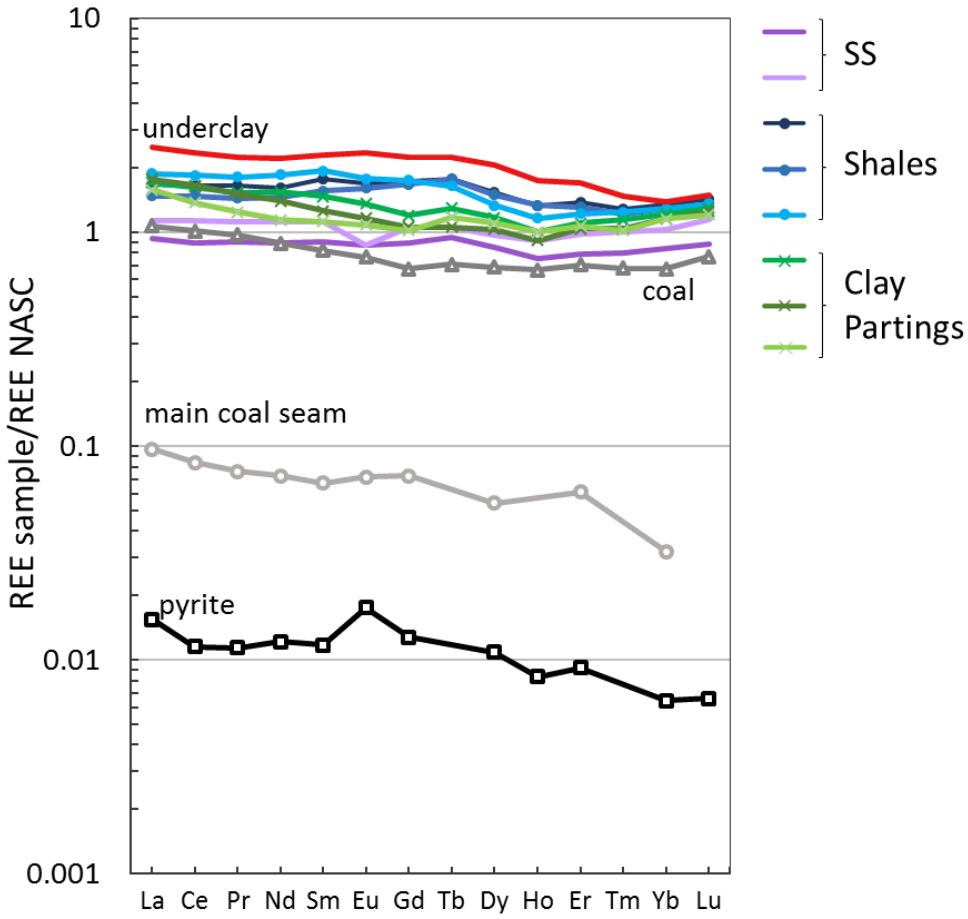

Figure 12. NASC-normalized REE patterns of whole rock, coal and pyrite samples from the lower Pittsburgh Formation.

4.1.3 Leachate samples

Geochemical data for all leachates are reported in Table 8 (major elements), Table 9 (trace elements), and Table 10 (REEs). REE concentrations in ammonium acetate leachates were below MDL for most units. Two samples with concentrations above detection limits exhibited a convex, MREE-enriched pattern (Figure 13). However, REE concentrations (µg REE leached per gram of sample) in leachates are lower than what would be expected to account for REE concentrations in AMD, since AMD is generated in a significantly more dilute environment.

Sulfuric acid leachates yielded higher REE concentrations for all samples except for the main coal seam (least mineral matter), which was below MDL for most REEs. The highest REE concentrations were found in the underclay leachate (TREE = 130 ppm), followed by the sandstones and shales of the overburden (TREE = 12-14 ppm). Other than the main coal seam (mostly below MDL), the lowest REE concentrations (TREE = 1.8 – 3.2 ppm) were found in leachates of the clay partings and mineral-rich coal. These concentrations are similar to the ammonium acetate leachates with the highest REE concentration (Figure 13). All sulfuric acid leachates, with the except of the main coal seam, exhibited a MREE-enriched pattern (Figure 13). It should be noted that although the underclay leachate shows the highest REE concentrations, its NASC-normalized concentration ratio (N) of La/Sm is greater than 1 $(La/Sm)_N>1$), indicating a less developed MREE-enriched pattern relative to the shales and sandstones of the overburden with $(La/Sm)_N < 1$ (Seredin and Dai 2012; Sun et al. 2012).

Table 8. Major element concentrations (µg/g leached) in leachate samples of the Pittsburgh Botanic Garden's stratigraphic section. Samples were measured by ICP-OES at Activation Laboratories, Canada.

Sample Leach	Description	Si	Al	Fe	Mg	Mn	Ca	Na	K	Ti	P
		(µg/g)									
Ammonium Acetate											
PBG-SS1	Sandstone	5.90	< 1.5	< 0.15	22.1	11.8	1520	5.90	42.8	< 0.15	0.295
PBG-15	Shale	4.55	1.52	< 0.15	256	9.41	809	36.4	349	< 0.15	0.304
PBG-13	Shale above coal	13.9	< 1.3	0.13	313	13.4	1104	22.8	232	< 0.13	0.380
PBG-9	Clay Parting	1.48	8.88	< 0.15	62.2	1.63	54.8	< 1.5	8.88	< 0.15	0.444
PBG-4	Coal	6.76	< 1.3	4.19	16.2	< 0.13	56.8	17.6	16.2	< 0.13	0.541
PBG-3	Clay Parting	< 1.4	1.38	0.138	68.9	1.38	103	15.2	132	< 0.14	< 0.28
PBG-1	Main Coal Seam	< 1.2	< 1.2	< 0.12	2.51	0.125	22.6	10.0	< 1.2	< 0.12	0.376
PBG-UC	Underclay	6.62	< 1.3	0.662	379	8.74	2146	30.5	395	< 0.13	5.96
Sulfuric Acid											
PBG-SS1	Sandstone	32.1	348	2767	479	109	3608	9.88	54.4	2.72	232
PBG-15	Shale	374	536	13780	594	465	1021	15.2	106	1.77	161
PBG-13	Shale above coal	70.0	299	4308	112	159	709	10.6	48.8	0.637	183
PBG-9	Clay Parting	83.9	800	783	19.8	3.70	7.41	< 2.5	17.3	0.494	83.9
PBG-4	Coal	40.6	94.7	643	6.76	0.451	15.8	2.25	9.02	0.676	18.0
PBG-3	Clay Parting	156	586	419	9.16	1.83	6.87	4.58	48.1	0.458	5.49
PBG-1	Main Coal Seam	< 2.1	6.28	120	2.09	< 0.21	8.37	< 2.1	< 2.1	< 0.21	1.05
PBG-UC	Underclay	193	667	729	102	16.2	18079	129	195	0.886	5915

Table 9. Trace element concentrations (μg/g leached) in leachate samples of the Pittsburgh Botanic Garden's stratigraphic section. Samples were measured by ICP-OES at Activation Laboratories, Canada.

Sample Leach	Ag	As	Ba	Be	Cd	Ce	Co	Cr	Cu	Li	Mo	Ni	Pb	S	Sb	Se	Sn	Sr	Te	Tl	U	V	W	Y	Zn
												(μg/g)													
Ammonium Acetate Leach																									
PBG-SS1	< 0.07	< 0.4	1.3	< 0.03	< 0.03	< 0.4	0.43	< 0.3	0.059	< 0.7	< 0.07	0.09	< 0.2	15	< 0.2	< 0.3	< 0.2	3.7	< 0.2	< 0.2	< 0.7	< 0.2	0.44	0.15	0.97
PBG-15	< 0.08	< 0.5	19	< 0.03	< 0.03	< 0.5	0.15	< 0.3	3.2	< 0.8	< 0.08	0.86	< 0.2	46	< 0.2	< 0.3	< 0.2	3.5	< 0.2	< 0.2	< 0.8	< 0.2	< 0.2	< 0.2	4.0
PBG-13	< 0.06	< 0.4	24	< 0.03	0.025	< 0.4	0.58	< 0.3	8.2	< 0.6	0.089	1.2	0.38	101	< 0.1	0.38	< 0.1	4.2	0.25	< 0.1	< 0.6	< 0.1	< 0.1	< 0.2	4.6
PBG-9	< 0.07	< 0.5	1.5	< 0.03	0.13	< 0.4	0.89	< 0.3	11	< 0.7	0.10	3.7	< 0.2	518	< 0.2	< 0.3	< 0.2	0.15	0.30	< 0.2	< 0.7	< 0.2	< 0.1	< 0.2	3.8
PBG-4	< 0.07	< 0.4	1.6	< 0.03	< 0.03	< 0.4	0.32	< 0.3	0.42	< 0.7	0.095	0.93	< 0.1	352	< 0.1	< 0.3	< 0.1	2.0	< 0.1	< 0.1	< 0.7	< 0.1	< 0.1	< 0.1	2.1
PBG-3	< 0.07	< 0.4	9.0	< 0.03	0.041	< 0.4	1.5	< 0.3	2.8	< 0.7	0.096	1.8	0.28	262	< 0.1	0.41	< 0.1	1.1	< 0.1	< 0.1	< 0.7	< 0.1	0.28	< 0.1	7.1
PBG-1	< 0.06	< 0.4	0.63	< 0.03	< 0.03	< 0.4	0.088	< 0.3	0.21	< 0.6	< 0.06	0.14	< 0.1	113	< 0.1	< 0.3	< 0.1	1.0	< 0.1	< 0.1	< 0.6	< 0.1	< 0.1	< 0.1	3.3
PBG-UC	< 0.07	< 0.4	24	< 0.03	0.040	< 0.4	3.8	< 0.3	10	< 0.7	0.13	12	< 0.1	1139	< 0.1	< 0.3	< 0.1	29	< 0.1	< 0.1	< 0.7	< 0.1	0.13	< 0.1	7.7
Sulfuric Acid Leach																									
PBG-SS1	< 0.1	1.2	1.7	0.049	0.25	2.7	6.3	0.74	0.25	< 1	< 0.1	1.6	4.2	13319	< 0.3	< 0.5	< 0.3	9.4	0.49	0.25	< 1	0.99	2.2	3.5	4.8
PBG-15	< 0.1	< 0.8	3.5	0.30	1.1	2.3	3.4	1.3	2.8	< 1	< 0.1	3.0	3.3	36915	0.76	< 0.5	< 0.3	4.0	1.8	0.76	1.3	4.8	< 0.3	4.0	12
PBG-13	< 0.1	1.1	4.2	0.45	0.40	2.8	9.1	0.64	18	< 1	< 0.1	7.6	8.3	10779	0.21	< 0.4	< 0.2	4.7	0.64	< 0.2	< 1	2.5	0.21	4.7	28
PBG-9	< 0.1	6.2	2.2	0.20	0.25	< 0.7	20	1.7	12	2.2	< 0.1	3.5	0.99	7728	< 0.3	< 0.5	< 0.3	0.25	0.49	< 0.3	< 1	1.2	< 0.3	0.49	15
PBG-4	< 0.1	2.9	0.90	< 0.05	0.068	1.1	2.7	< 0.5	1.9	< 1	< 0.1	2.1	1.8	5772	< 0.2	< 0.5	< 0.2	0.68	< 0.2	< 0.2	< 1	0.45	< 0.2	< 0.2	7.4
PBG-3	< 0.1	3.9	2.7	0.21	0.14	< 0.7	18	0.46	5.7	1.6	< 0.1	4.3	5.3	8494	< 0.2	< 0.5	< 0.2	0.46	< 0.2	< 0.2	< 1	0.69	0.46	0.69	43
PBG-1	< 0.1	< 0.6	0.42	< 0.04	< 0.04	< 0.7	0.15	< 0.4	0.52	< 1	< 0.1	0.17	< 0.2	2385	< 0.2	< 0.4	< 0.2	< 0.2	< 0.2	< 0.2	< 1	< 0.2	< 0.2	< 0.2	1.3
PBG-UC	< 0.1	4.9	5.8	0.49	0.13	36	9.1	0.66	10	< 1	0.22	7.0	2.4	27694	< 0.2	< 0.4	< 0.2	187	0.44	< 0.2	< 1	0.44	< 0.2	28	25

Table 10. REE concentrations (µg/kg leached) in leachate samples of the Pittsburgh Botanic Garden's stratigraphic section. Samples were measured by ICP-MS at the University of Pittsburgh.

Sample	Description	La	Ce	Pr	Nd	Sm	Eu	Gd	Tb	Dy	Ho	Er	Tm	Yb	Lu	TREE
									µg/kg							
Ammonium Acetate Leach																
PBG-SS1	Sandstone	72.6	176	28.4	143	64.9	21.7	87.1	14.0	74.0	15.2	39.2	< 4.8	28.5	4.06	
PBG-15	Shale	< 3.5	< 6.2	< 1.4	< 1.8	< 6.2	< 2.1	< 3.1	< 0.78	< 2.6	< 0.80	< 2.1	< 0.22	< 1.3	< 0.27	
PBG-13	Shale above coal	< 4.6	< 7.5	< 0.78	< 7.0	< 0.45	< 1.4	6.01	< 0.74	< 5.0	< 0.73	< 2.7	< 0.14	< 1.3	< 0.055	
PBG-9	Clay Parting	< 3.6	< 6.6	< 0.97	< 2.6	< 4.4	< 2.9	6.17	< 0.71	< 4.4	< 0.38	< 0.74	< 0.076	0.00	0.00	
PBG-4	Coal	< 3.5	9.75	< 1.0	< 5.4	< 1.3	< 0.51	< 1.9	< 0.061	< 0.83	< 0.21	< 0.52	< 0.031	< 0.37	< 0.043	
PBG-3	Clay Parting	42.2	104	17.9	107	26.0	< 6.8	37.4	< 4.4	< 16	< 3.2	< 6.3	< 0.54	< 3.2	< 0.22	
PBG-1	Main Coal Seam	< 0.74	< 2.0	< 0.20	< 0.81	< 0.50	0.00	< 0.16	< 0.073	0.00	0.00	0.00	0.00	< 0.059	0.00	
PBG-UC	Underclay	< 0.75	< 2.1	< 0.47	< 1.5	0.00	< 0.15	< 0.17	< 0.080	< 0.60	< 0.11	< 0.80	< 0.017	< 0.25	0.00	
Sulfuric Acid Leach																
PBG-SS1	Sandstone	1033	3452	553	2865	989	261	1196	175	957	174	442	63.3	374	51.2	12585
PBG-15	Shale	791	3156	534	3312	1462	376	2020	276	1175	187	415	50.4	257	38.0	14051
PBG-13	Shale above coal	896	3542	572	3288	1370	388	2048	283	1409	224	512	62.7	352	46.4	14994
PBG-9	Clay Parting	98.5	403	77.1	481	182	47.1	213	25.8	157	26.3	76.1	< 9.9	52.2	7.68	1858
PBG-4	Coal	405	1372	177	758	172	35.8	152	18.8	82.3	12.2	25.5	< 2.8	17.9	1.85	3235
PBG-3	Clay Parting	164	695	117	570	168	45.7	269	44.9	258	46.8	121	< 15.0	102	14.2	2633
PBG-1	Main Coal Seam	19.6	44.1	< 5.4	18.3	< 5.5	< 1.2	< 5.0	< 0.43	< 2.4	< 0.31	< 0.72	< 0.07	< 0.60	< 0.22	
PBG-UC	Underclay	15052	48110	6861	29641	7088	1633	7846	1160	6667	1209	2794	311	1493	172	130035

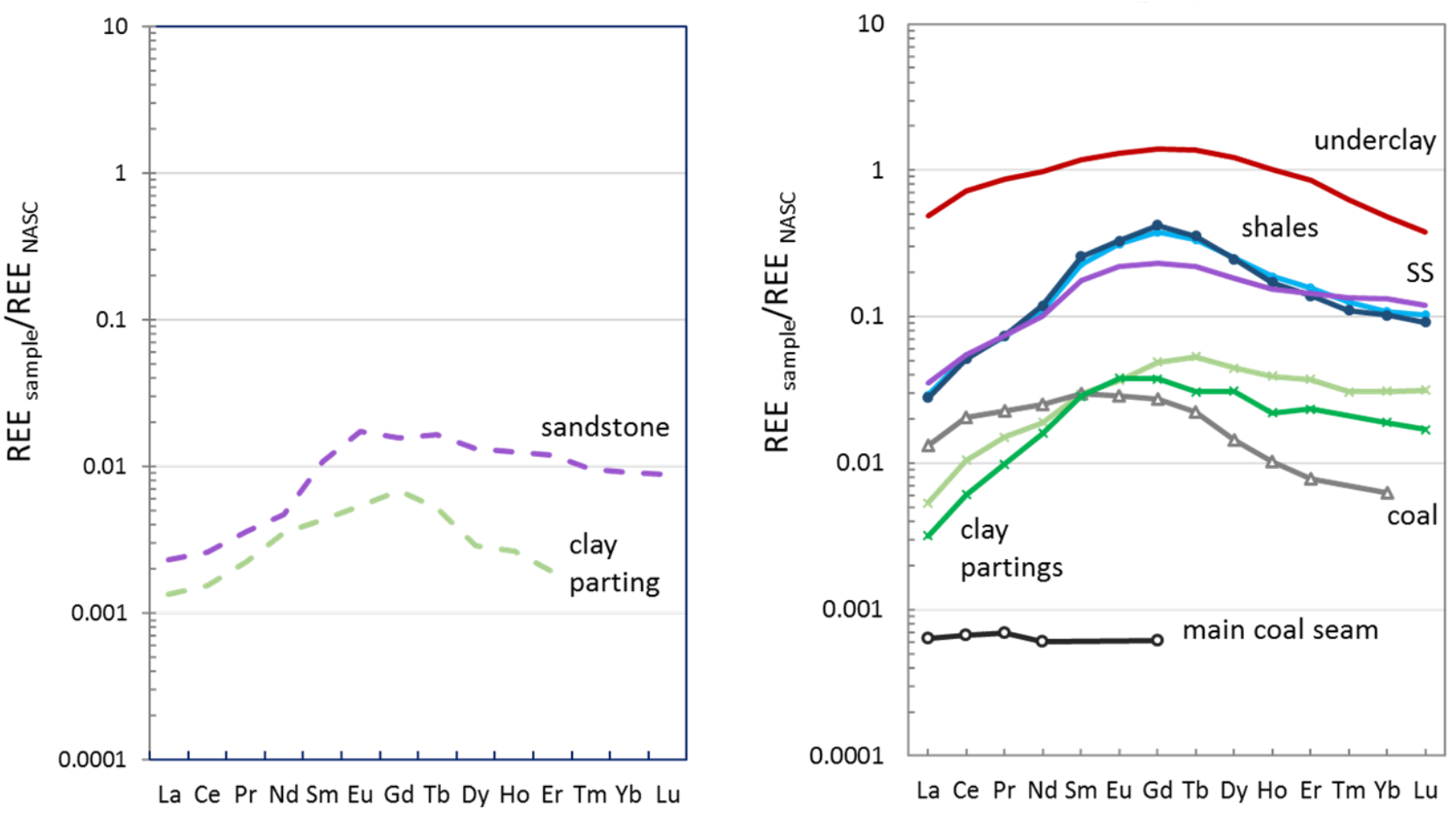

Figure 13. NASC-normalized REE patterns for ammonium acetate leachates (left) and sulfuric acid leachates (right) of rock units adjacent to the Pittsburgh Coal in the lower Pittsburgh Formation.

4.2 NEODYMIUM ISOTOPE GEOCHEMISTRY

Samarium and neodymium concentrations and neodymium isotope data for selected whole rock samples, ammonium acetate leachates, and sulfuric acid leachates are presented in Table 11. $^{143}Nd/^{144}Nd$ ratios are reported in epsilon notation where ε_{Nd} at time (T) is given by:

$$\varepsilon_{Nd}(T) = 10^4 \left(\frac{^{143}Nd/^{144}Nd\ (T)_{sample}}{^{143}Nd/^{144}Nd\ (T)_{CHUR}} - 1 \right)$$

Epsilon notation reports the isotopic ratio relative to the chondritic uniform reservoir (CHUR), a proxy for bulk earth at time (T) in years before present. Time (T) is generally the age of formation, whereas $\varepsilon_{Nd}(0)$ is the measured value at present day (DePaolo and Wasserburg 1976).

All measured $\varepsilon_{Nd}(0)$ values for selected whole rock units adjacent to the Pittsburgh Coal (Table 11), leachates (Table 11) and AMD (Table 12) are negative, consistent with an older continental crust source. Whole rock $\varepsilon_{Nd}(0)$ values (-11.3 to -12.2) agree with reported $\varepsilon_{Nd}(0)$ values for Pennsylvanian age strata of Western PA (Schatzel and Stewart 2012). Additionally, when corrected back to an approximate age of sedimentation (300 Ma) whole rock $\varepsilon_{Nd}(T)$ values are in the range of $\varepsilon_{Nd}(T)$ values reported for Appalachian Basin strata by Patchett, Ross, and Gleason (1999). However, regional mine drainage from the Pittsburgh Coal is notably more radiogenic ($\varepsilon_{Nd}(0)$ between -8.0 to -9.1) than the local strata with which AMD interacts. Most leachate $\varepsilon_{Nd}(0)$ values ranged from -5.8 to -9.3, straddling the $\varepsilon_{Nd}(0)$ range of Pittsburgh Coal AMD (Figure 14). The underclay leachate was anomalous with a $\varepsilon_{Nd}(0)$ of -11.0, which was closer to whole rock values.

Table 11. Nd isotope data for whole rock and leachate samples of the Pittsburgh Botanic Garden's stratigraphic section, Pittsburgh, PA. Isotope data determined by TIMS at the University of Pittsburgh.

Sample	Description	147Sm/ 144Nd	εNd(0)[1]	εNd(300Ma)[2]
Whole Rock				
PA-PBG-SS1	Sandstone	0.1192	-11.18 ± 0.12	-8.21 ± 0.27
PA-PBG-3	Clay Parting	0.1164	-12.02 ± 0.16	-8.94 ± 0.31
PA-PBG-UC	Underclay	0.1231	-11.53 ± 0.12	-8.72 ± 0.26
Ammonium Acetate Leach				
PA-PBG-SS1	Sandstone	0.2747	-5.78 ± 0.14	-8.78 ± 0.29
PA-PBG-3	Clay Parting	0.1462	-8.09 ± 0.14	-6.15 ± 0.23
Sulfuric Acid Leach				
PA-PBG-SS1	Sandstone	0.2088	-6.10 ± 0.20	-6.57 0.22
PA-PBG-15	Shale	0.2669	-7.13 ± 0.12	-9.83 0.25
PA-PBG-13	Shale above coal	0.2520	-6.23 ± 0.12	-8.36 0.22
PA-PBG-9	Clay Parting	0.2288	-6.80 ± 0.12	-8.04 0.18
PA-PBG-4	Coal	0.1375	-9.28 ± 0.12	-7.01 0.23
PA-PBG-3	Clay Parting	0.1777	-7.87 ± 0.14	-7.15 ± 0.17
PA-PBG-OA	Underclay	0.1446	-11.02 ± 0.16	-9.03 ± 0.26

[1] $^{143}Nd/^{144}Nd_{CHUR}=0.511847$

[2] $^{147}Sm/^{144}Nd_{CHUR}=0.1967$

Table 12. Nd isotope data for Pittsburgh Coal mine discharges in Western, PA. Samples measured by TIMS at the University of Pittsburgh.

Pittsburgh Coal Discharges	Sample Date	147Sm/ 144Nd	εNd(0)[1]
IB-Export	3/3/1999	0.1899	-8.65 ± 0.14
IB-Delmont	3/3/1999	0.2044	-8.19 ± 0.25
CH-McLaughlin	2/28/2002		-7.97 ± 0.23
CH-Whiskey Run	2/28/2002	0.1803	-8.67 ± 0.31
CH-Presto Sygan	2/28/2002	0.1707	-8.83 ± 0.14
CH-Hope Hollow	2/28/2002	0.2057	-8.05 ± 0.2
CH-Botanical Garden	2/28/2002	0.1869	-8.83 ± 0.33
Pittsbugh Botanic Garden	12/10/2016		-9.12 ± 0.57

[1] $^{143}Nd/^{144}Nd_{CHUR}=0.511847$

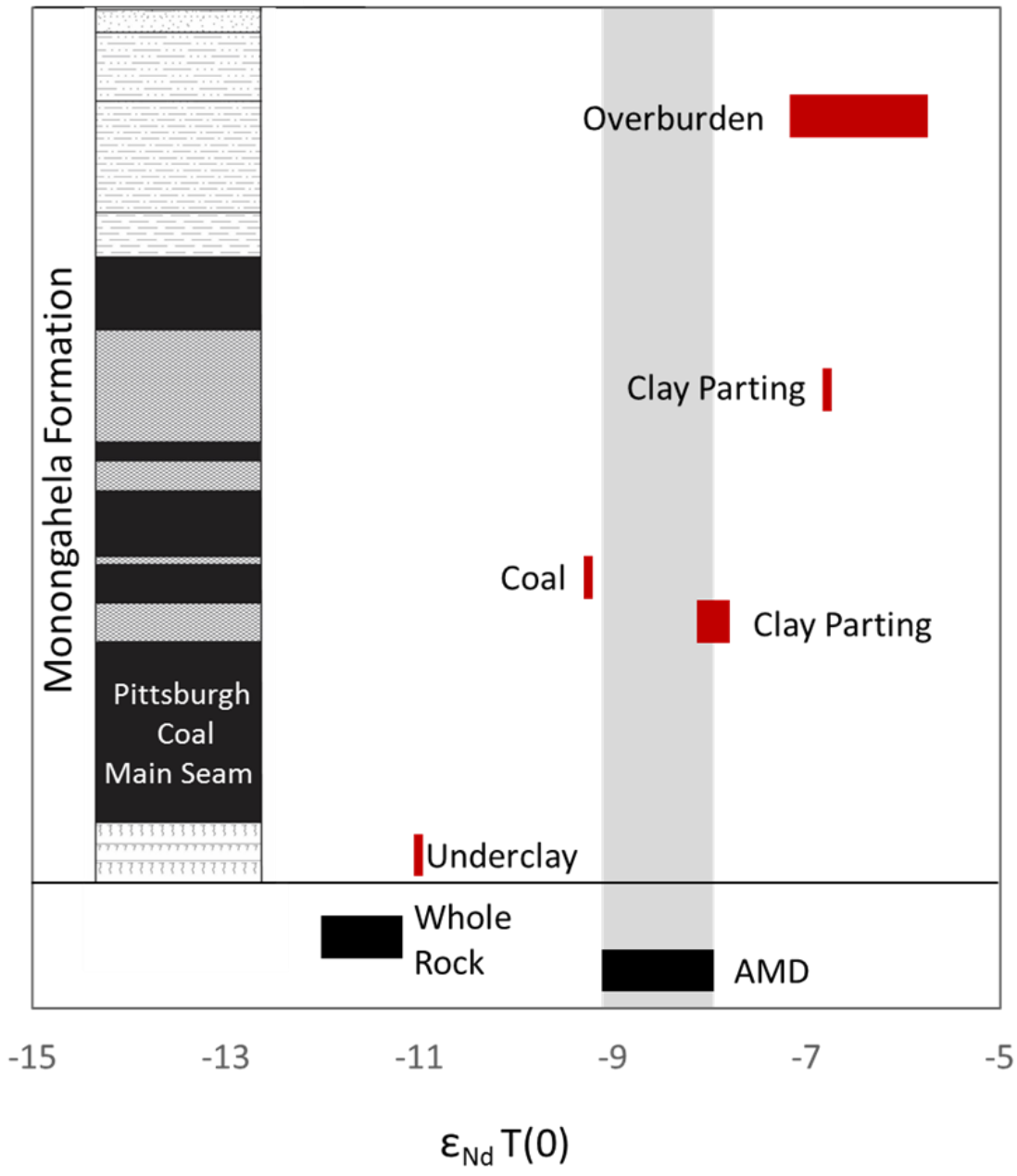

Figure 14. ε_{Nd} values of whole rock leachates compared to Pennsylvanian strata of the lower Pittsburgh Formation and Pittsburgh Coal AMD from Western, PA. AMD from the Pittsburgh Coal is more radiogenic than Pennsylvanian strata from Appalachian Basin. ε_{Nd} values for leachates also show a more radiogenic isotopic signature, straddling the AMD ε_{Nd} range. This suggests the Nd signature, of AMD is a result of preferential leaching of a high Sm/Nd phase mineral(s) within the whole rock.

A pseudo-isochron for this system was created by plotting whole rock and leachate $^{143}Nd/^{144}Nd$ vs $^{147}Sm/^{144}Nd$ data. A best fit line was generated, the slope of which suggests an approximate age of 320 $\pm$ 98 Ma (Figure 15). This approximate age of formation (T) for the Nd sources in theses samples falls within the mid-Carboniferous Period, more specifically the lower Pennsylvanian (~315 – 323 Ma)(Cohen 2013). The general agreement between the calculated age and known depositional age of the Pittsburgh Coal argues against this being a simple mixing relationship.

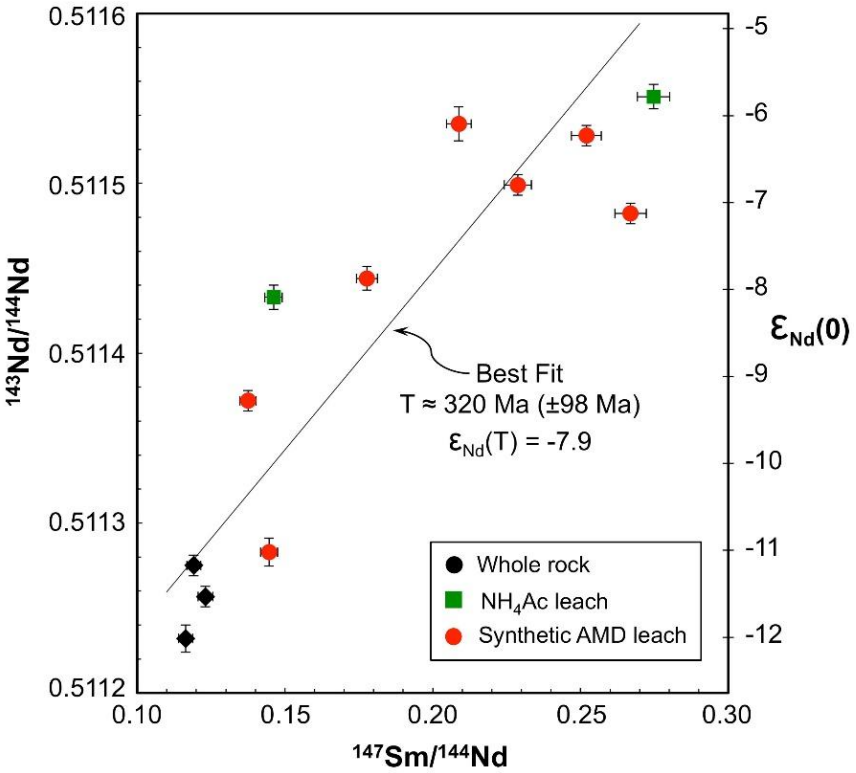

Figure 15. PBG pseudo-isochron generated from whole rock (black circles), ammonium acetate leachate (green squares), and sulfuric acid leachate (red circles) Sm-Nd data (143Nd/144Nd vs 147Sm/144Nd). Slope of best fit line approximates time T (320Ma $\pm$ 98).

5.0 DISCUSSION

5.1 SOLID PHASE CONTROLS ON REES IN AMD

5.1.1 Colloidal Controls on REEs in AMD

Colloids are reactive solids (0.45 μm to 1 nm) that stay in suspension and behave differently than dissolved constituents (Gardner and Apul 2002). They are a significant transport mechanism in aqueous systems, controlling the mobility and distribution of reactive metals that sorb to their surfaces (Gustafsson and Gschwend 1997; Gardner and Apul 2002). Groundwater and surface water studies (pH range from 4.4 to 7.5) have shown a directly proportional relationship between REE concentrations and filter size (Viers et al. 1997; Dia et al. 2000; Ingri et al. 2000; Åström and Corin 2003). In these studies, the decrease in REE concentrations between unfiltered and filtered (0.45μm to 0.025μm) samples, and the decrease in REE concentrations between filtered and ultra-filtered (100 kDa to 3 kDa) samples, supports the strong influence of organic matter and colloids on REE transport and chemical behavior in natural waters (filter size varied by study). Dia et al. (2000) reported that 40–60% of REEs were transported and controlled by the colloidal fraction in natural aqueous environments. Ingri et al. (2000) also reported similar percentages.

As a majority of REE transport can be attributed to colloid mobility in some aqueous systems, the degree of colloidal interaction must be determined in order to understand REE behavior in a given system. It is especially important to determine if REEs exist as stable aqueous complexes, or if they have partitioned into the solid phase, when using REE patterns to interpret geochemical processes (Verplanck 2013). This is due to the systematic variation in reactivity along the REE series, with HREEs and MREEs having a greater affinity for the solid-phase than the LREEs (this relationship generally exists at higher pH) (Sun et al. 2012; Verplanck 2013). If REE are reacting with colloids, then the REE patterns yielded will be a product of colloid reactivity and transport *and* water-rock interaction within the system. For this reason, unfiltered samples and three filtered samples (from 0.45 µm to 0.22 µm to 3kDa molecular weight cutoff (MWCO)) of Pittsburgh Coal mine discharges were collected at each mine drainage site.

Unlike previously discussed studies of natural waters, successive filtration of Pittsburgh Coal acidic discharges yielded little to no change in REE concentrations relative to unfiltered samples (Figure 10). AMD filtration data from this study supports previous studies that have found REEs to be completely, or nearly completely, dissolved in mine drainage with pH < 5.1 (Verplanck et al. 2004; Verplanck 2013). This supports the use of REE as tracers of water-rock interactions in acidic systems like the PBG, as misinterpretations due to unknown partitioning behavior are less likely (Verplanck 2013).

5.1.2 Oxyhydroxide precipitate controls on REEs in AMD

The TREE concentration and pH of Pittsburgh Coal mine drainage are inversely related (REE concentration decreases as pH increases), and when mine discharges reach circumneutral

pH (pH $\geq$ 5.1) REE concentrations decrease sharply (Table 3 and 4). Several studies have observed similar pH dependent REE behavior in aqueous systems (Leybourne et al. 2000; Andersson et al. 2001; Åström 2001; Verplanck et al. 2004; Olías et al. 2005; Welch et al. 2009; Verplanck 2013). The drastic decrease in REE concentrations at circumneutral pH has been attributed to sorption to the solid phase - notably oxide and hydroxide precipitates (Serrano, Sanz, and Nordstrom 2000; Coppin et al. 2002; Verplanck et al. 2004; Gammons et al. 2005; Verplanck 2013; Xu and Han 2009). The similar pH dependent trend seen in Al concentrations (Table 2) in Pittsburgh Coal mine drainage suggests that Al oxyhydroxides (Nordstrom and Ball 1986) may be the dominant solid phase preferential scavenging REEs in the circumneutral Irwin Basin discharges (pH > 5.1). Thus, at higher pH REEs are more reactive in this system, partitioning to the solid phase.

5.2 PREFERENTIAL DISSOLUTION OF DISCRETE MINERAL PHASES AS A SOURCE OF MREE ENRICHMENT

As noted by Worrall and Pearson (2001), AMD exhibits a shale normalized MREE-enriched pattern that is dissimilar to that of the local strata with which these fluids interact. Yet, when these same rock units are leached, the resulting leachates exhibits similar MREE-enriched patterns to what is seen in AMD. Whole rock and leachate data from this study support these findings (Figure 16). This suggests that REEs in AMD originates from discrete phases within the rock units that are preferentially dissolved in dilute acid, rather than from whole rock dissolution. Other studies (Worrall and Pearson 2001; Merten and Buchel 2004; Leybourne and Cousens 2005; Merten et al. 2005; Wood, Shannon, and Baker 2005; Sun et al. 2012) have proposed

preferential dissolution of MREE-enriched mineral phases within the bedrock as the source for MREE-enrichment in acidic waters.

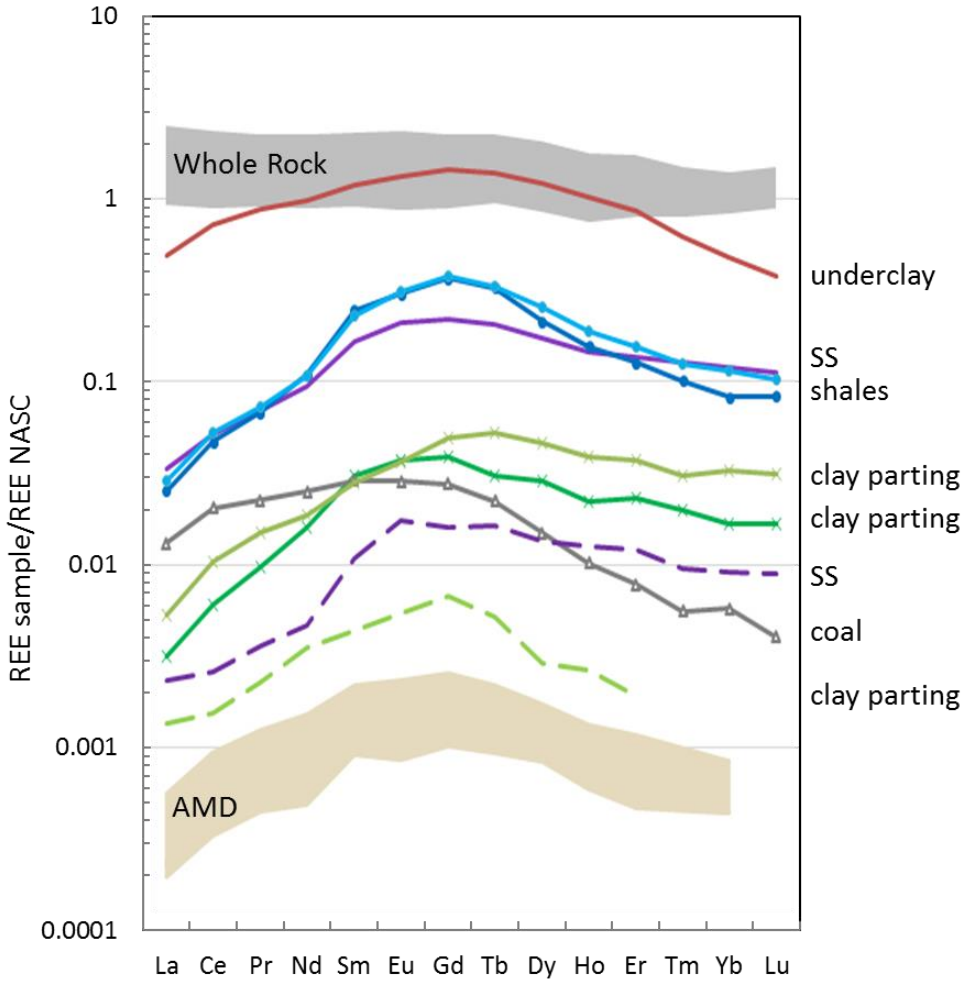

Figure 16. Compilation of NASC-normalized REE patterns of study samples. Ammonium acetate leachates (dashed lines) and sulfuric acid leachates (solid lines) of whole rock samples adjacent to the Pittsburgh Coal in the lower Pittsburgh Formation exhibit a MREE-enrichment pattern. This is similar to the NASC-normalized REE patterns of Pittsburgh Coal AMD (shaded in tan). Conversely, NASC-normalized whole rock REE patterns (shaded gray) are

In this study, sulfuric acid leachates of the whole rock samples yielded similar MREE-enriched patterns and ε_{Nd} (0) values as those observed in AMD, distinct from bulk rock REE patterns and ε_{Nd} (0) values. This supports the use sulfuric acid leaches as reasonable proxies for

the fluid-rock interactions in an AMD systems. Additionally, the more radiogenic $\varepsilon_{Nd}(0)$ values of the leachates, relative to whole rock samples, further supports preferential dissolution of a discrete mineral phase(s) in the regional strata as a primary source of MREE-enrichment in AMD. This suggests the leaching of a relatively high Sm/Nd ratio mineral phase in the siliciclastic units surrounding the coal seam.

The less radiogenic signature of the underclay leachate ($\varepsilon_{Nd}(0) = -11$) suggests that this unit experiences a higher degree of whole rock dissolution relative to the other siliciclastic units in the section, which appear to experience preferential leaching of discrete phases when exposed to acidic leaching conditions. This interpretation is further supported by the high percentage of TREEs removed from the bulk rock by the leach (>30%), and the less developed MREE-enriched pattern $(La/Sm)_N > 1$. This unit still may be a major contributor of REEs to AMD. Since this is not a closed system in nature, the isotopic signature of Pittsburgh Coal mine drainage likely results from interactions with multiple units (i.e. mixing between a less radiogenic underclay leachate and a more radiogenic overburden leachate). Therefore, units which yielded high concentrations of MREEs when leached are most likely dominant contributors to the REE concentrations and signatures seen in AMD.

5.3 PHASES CONTRIBUTING TO REE PATTERNS OF AMD

The general trend of the leachate data along the best fit line of the pseudo-isochron (Figure 9), suggests the source of Nd in the leachates was present during deposition and diagenesis, and not formed during a later stage alteration event. Regression calculations also support a REE source that is syngenetic to these stratigraphic units (coeval to deposition), rather

than a polygenetic/multistage hydrothermal origin (Seredin and Chekryzhov 2011). Additionally, the low REE concentration of the main seam coal sample (2.61% ash) relative to the more mineral-rich coal sample (49.7% ash), suggests a mineral origin for REEs rather than an organic compound association (Seredin and Dai 2012). The source of REEs, and ultimately MREE-enriched patterns, in AMD appears to be a mineral phase present at the time of deposition that is readily dissolvable in dilute acid, with high total REE concentrations, and a Sm/Nd greater than the bulk rock.

Apatite is one such mineral that yields MREE-enriched patterns (Joosu et al. 2016). It has been suggested as a potential source for the MREE-enriched patterns found in studies of acidic natural waters (Aubert, Stille, and Probst 2001; Hannigan and Sholkovitz 2001; García et al. 2007). Petrographic analysis of the Pittsburgh Coal stratigraphic section supports the possible presence of apatite in the shale overburden.

Mass balance calculations using a range of Nd concentrations for Apatite (300-1300 ppm) (Nagasawa 1970; Comodi et al. 1999; Aubert, Stille, and Probst 2001) were used to test the plausibility of apatite as a potential source in this system. Calculations yielded theoretical estimates of how much Nd apatite could contribute to each leachate, assuming all phosphorous in the leachates (Table 8) resulted from apatite dissolution. Assuming apatite with a low Nd concentration (300 ppm), calculations estimate that 10-30% of the Nd present in overburden shale and sandstone unit leachates could be accounted for by apatite dissolution. The same calculation, assuming the presence of apatite with higher Nd concentrations (1300 ppm), estimates that 40-60% of the Nd present in those same leachates could be accounted for by apatite dissolution. Similar calculations for the clay units within the coal seam were not possible. Stoichiometrically, there was not enough Ca in these leachates for all P to be generated from

apatite, assuming that for each mole of apatite there are 5 moles of Ca and 3 moles of P. Thus, the assumption that all phosphorus present in the leachates was from apatite dissolution was invalidated for those units.

Carbonate minerals/cements also meet the above mentioned criteria and can exhibit MREE-enriched patterns (Phan et al. 2017). There are several non-marine to marginal-marine limestone units in the Conemaugh and Monongahela groups (Arkle 1974; Ruppert et al. 1999; Karacan 2009) making it a reasonable potential source of REEs in this system. However, it should be noted, no limestone units were present at the sampling site, and none of the whole rock samples analyzed showed evidence of carbonate cement. In addition to apatite and carbonate minerals, there are several REE-rich accessory minerals from the phosphate and oxide (Gunn 2014) mineral families, which cannot be ruled out as potential sources of REE at this time.

Pyrite has also been proposed as a potential source of MREE-enrichment in AMD (Grawunder, Merten, and Buchel 2014). Grawunder et al. (2014) reported a pronounced MREE-enriched pattern when pyrite was leached with sulfuric acid. The authors postulate that MREE mobilization by S-species complexation during pyrite oxidation in low pH environments could account for the common REE pattern found in AMD. However, additional mass balance calculations with sulfur data from this study show that the low REE concentrations in pyrite make it a highly improbable source of REE enrichment.

The amount (g) of pyrite need to generate an average sulfur concentration of 171 mg (Table 1) in 1 L of AMD was determined using the assumption that two moles of sulfate are released for every mole of pyrite dissolved (Eq. 1). This theoretical amount of pyrite (approximately 0.32 g) allowed us to determine the amount of TREEs pyrite would release per liter of AMD, assuming a TREE concentration of 2 μg/g for pyrite (Table 7). In this scenario,

pyrite would generate 0.64 μg/L TREE, which is less than 0.4% of the TREE found in PBG AMD (average TREE concentration = 180 μg/g) (Table 2). Even when the calculation was repeated assuming a higher TREE concentration for pyrite (66 μg/g: the highest concentration reported in Grawunder (2014), the contribution of pyrite to the TREEs found in the PBG system would be approximately 10%.

6.0 CONCLUSIONS

The evidence put forth in this study supports a source derived origin for MREE-enrichment in AMD and provides geochemical and isotopic constraints on mineral phases in the local substrate contributing REE to AMD. Filtration data indicates REEs in acidic (pH < 5.1) coal mine drainages are fully dissolved, not bound to particles or colloids. This argues against process driven colloidal controls as a mechanism for enrichment and further supports the interpretation of REE data as a tracer of source.

REE patterns of AMD are inconsistent with whole rock dissolution of the local strata. However, the generation of MREE-enrich patterns in laboratory leaching experiments implies MREE-enrichment is derived from discrete mineral phases within these rock units, further supporting a source derived origin for MREE-enrichment in Pittsburgh Coal AMD. Additionally, REE patterns of these leachates suggest that mineral phases within the siliciclastic overburden units are primary contributors of REE concentrations and MREE-enrichment in this system.

Preferential dissolution is further supported by Nd isotope data. ε_{Nd} (0) values for most leachates (-5.8 to -9.3) were similar to AMD values (-8.0 to -9.1), and were more radiogenic than the whole rock samples being leached (-11.3 to -12.2). This indicates that Nd in the leachates results from the preferential dissolution of mineral phases with a higher Sm/Nd ratios than the bulk rock. The similar ε (0) values for leachates and AMD samples supports a similar Nd source in AMD systems. Additionally, regression calculations corrected to a late-Carboniferous

depositional age support a Nd source present at the time of deposition, which has not chemically interacted with the bulk rock during a later stage alteration event.

Geochemical and isotopic data suggests an AMD Nd (and therefore other REE) source derived from preferential leaching/dissolution of discrete high Sm/Nd, MREE-enriched mineral phases in local rock units. As mass balance calculations show, pyrite is an improbably source. Possible mineral phases with high REE concentrations and high Sm/Nd ratios, which are readily dissolved in dilute acid, include apatite and other phosphate minerals, carbonate minerals and cements, and other accessory minerals. An understanding of REE source and mobility in AMD systems will allow researchers to more effectively target promising locations for REE resource recovery in the future. This study emphasizes the importance of geochemical and mineralogical characterizations of local rock units to properly assess site potential.

BIBLIOGRAPHY

Akcil, A., and S. Koldas. 2006. Acid Mine Drainage (AMD): causes, treatment and case studies. *Journal of Cleaner Production* 14 (12-13):1139-1145.

Andersson, P. S., R. Dahlqvist, J. Ingri, and Ö. Gustafsson. 2001. The isotopic composition of Nd in a boreal river: a reflection of selective weathering and colloidal transport. *Geochimica et Cosmochimica Acta* 65 (4):521-527.

Arkle, T. 1974. Stratigraphy of the Pennsylvanian and Permian systems of the central Appalachians. *Geological Society of America Special Papers* 148:5-30.

Åström, M. 2001. Abundance and fractionation patterns of rare earth elements in streams affected by acid sulphate soils. *Chemical Geology* 175 (3):249-258.

Åström, M., and N. Corin. 2003. Distribution of rare earth elements in anionic, cationic and particulate fractions in boreal humus-rich streams affected by acid sulphate soils. *Water research* 37 (2):273-280.

Aubert, D., P. Stille, and A. Probst. 2001. REE fractionation during granite weathering and removal by waters and suspended loads: Sr and Nd isotopic evidence. *Geochimica et Cosmochimica Acta* 65 (3):387-406.

Ayora, C., F. Macías, E. Torres, and J. M. Nieto. 2015. Rare Earth Elements in Acid Mine Drainage. In *XXXV Reunión de la Sociedad Española de Mineralogía*. Huelva.

Binnemans, K., P. T. Jones, B. Blanpain, T. Van Gerven, Y. Yang, A. Walton, and M. Buchert. 2013. Recycling of rare earths: a critical review. *Journal of Cleaner Production* 51:1-22.

Blowes, D. W., C. J. Ptacek, J. L. Jambor, C. G. Weisener, D. Paktunc, W. D. Gould, and D. B. Johnson. 2014. 11.5 - The Geochemistry of Acid Mine Drainage A2 - Holland, Heinrich D. In *Treatise on Geochemistry (Second Edition)*, ed. K. K. Turekian, 131-190. Oxford: Elsevier.

Braun, J. J., and M. Pagel. 1990. U, Th and REE in the Akongo lateritic profile (SW Cameroon). *Chemical Geology* 84 (1):357-359.

Castle, J. 2001. Appalachian basin stratigraphic response to convergent-margin structural evolution. *Basin Research* 13 (4):397-418.

Cecil, C. B. 1990. Paleoclimate controls on stratigraphic repetition of chemical and siliciclastic rocks. *Geology* 18 (6):533-536

Cecil, C. B., R. W. Stanton, S. G. Neuzil, F. T. Dulong, L. F. Ruppert, and B. S. Pierce. 1985. Paleoclimate controls on late Paleozoic sedimentation and peat formation in the central Appalachian Basin (USA). *International Journal of Coal Geology* 5 (1-2):195-230

Cohen, K. M., Finney, S.C., Gibbard, P.L. & Fan, J.-X. 2013. The ICS International Chronostratigraphic Chart. Episodes 36: 199-204.

Commission, E. 2014. Report on Critical Raw materials for the EU. *Retrieved April* 30:2015.

Comodi, P., Y. Liu, F. Stoppa, and A. Woolley. 1999. A multi-method analysis of Si-, S-and REE-rich apatite from a new find of kalsilite-bearing leucitite (Abruzzi, Italy). *Mineralogical Magazine* 63 (5):661-672.

Coppin, F., G. Berger, A. Bauer, S. Castet, and M. Loubet. 2002. Sorption of lanthanides on smectite and kaolinite. *Chemical Geology* 182 (1):57-68.

Cravotta, C. A. 2008a. Dissolved metals and associated constituents in abandoned coal-mine discharges, Pennsylvania, USA. Part 1: Constituent quantities and correlations. *Applied Geochemistry* 23 (2):166-202.

Cravotta, C. A. 2008b. Dissolved metals and associated constituents in abandoned coal-mine discharges, Pennsylvania, USA. Part 2: geochemical controls on constituent concentrations. *Applied Geochemistry* 23 (2):203-226.

Czebiniak, M. 2016. Pittsburgh Botanic Garden brims with life after abandoned mine cleanup. *The Tribune-Review* October 24, 2016.

DePaolo, D., and G. Wasserburg. 1976. Nd isotopic variations and petrogenetic models. *Geophysical Research Letters* 3 (5):249-252.

Dia, A., G. Gruau, G. Olivié-Lauquet, C. Riou, J. Molénat, and P. Curmi. 2000. The distribution of rare earth elements in groundwaters: assessing the role of source-rock composition, redox changes and colloidal particles. *Geochimica et Cosmochimica Acta* 64 (24):4131-4151.

DOE, U. S. D. o. E. *Critical Materials Strategy* 2011 [cited.

Donaldson, A. C. 1974. Pennsylvanian sedimentation of central Appalachians. *Geological Society of America Special Papers* 148:47-78.

Edmunds, W. E., V. W. Skema, and N. K. Flint. 1999. Pennsylvanian. *The Geology of Pennsylvania—Special Publication* 1.

EIA, U. S. 2016. Annual Coal Report 2015.

Elderfield, H., R. Upstill-Goddard, and E. Sholkovitz. 1990. The rare earth elements in rivers, estuaries, and coastal seas and their significance to the composition of ocean waters. *Geochimica et Cosmochimica Acta* 54 (4):971-991.

Faill, R. T. 1997. A geologic history of the north-central Appalachians; Part 1, Orogenesis from the Mesoproterozoic through the Taconic Orogeny. *American Journal of Science* 297 (6):551-619.

Franus, W., M. M. Wiatros-Motyka, and M. Wdowin. 2015. Coal fly ash as a resource for rare earth elements. *Environ Sci Pollut Res Int* 22 (12):9464-74.

Gammons, C. H., S. A. Wood, J. P. Jonas, and J. P. Madison. 2003. Geochemistry of the rare-earth elements and uranium in the acidic Berkeley Pit lake, Butte, Montana. *Chemical Geology* 198 (3):269-288.

Gammons, C. H., S. A. Wood, and D. A. Nimick. 2005. Diel behavior of rare earth elements in a mountain stream with acidic to neutral pH. *Geochimica et Cosmochimica Acta* 69 (15):3747-3758.

Gammons, C. H., S. A. Wood, F. Pedrozo, J. C. Varekamp, B. J. Nelson, C. L. Shope, and G. Baffico. 2005. Hydrogeochemistry and rare earth element behavior in a volcanically acidified watershed in Patagonia, Argentina. *Chemical Geology* 222 (3-4):249-267.

García, M. G., K. L. Lecomte, A. I. Pasquini, S. M. Formica, and P. J. Depetris. 2007. Sources of dissolved REE in mountainous streams draining granitic rocks, Sierras Pampeanas (Córdoba, Argentina). *Geochimica et Cosmochimica Acta* 71 (22):5355-5368.

Gardner, K. H., and D. S. Apul. 2002. Influence of colloids and sediments on water quality. *Environmental and Ecological Chemistry* 2:264-277.

Gimeno Serrano, M. a. J., L. F. Auqué Sanz, and D. K. Nordstrom. 2000. REE speciation in low-temperature acidic waters and the competitive effects of aluminum. *Chemical Geology* 165 (3–4):167-180.

Grawunder, A., D. Merten, and G. Buchel. 2014. Origin of middle rare earth element enrichment in acid mine drainage-impacted areas. *Environ Sci Pollut Res Int* 21 (11):6812-23.

Greb, S. F., J. C. Pashin, R. L. Martino, and C. F. Eble. 2008. Appalachian sedimentary cycles during the Pennsylvanian: Changing influences of sea level, climate, and tectonics. *Geological Society of America Special Papers* 441:235-248.

Gunn, G. 2014. *Critical metals handbook*: John Wiley & Sons.

Gustafsson, C., and P. M. Gschwend. 1997. Aquatic colloids: concepts, definitions, and current challenges. *Limnology and Oceanography* 42 (3):519-528.

Hannigan, R. E., and E. R. Sholkovitz. 2001. The development of middle rare earth element enrichments in freshwaters: weathering of phosphate minerals. *Chemical Geology* 175 (3–4):495-508.

Hatcher, R. D. 2010. The Appalachian orogen: A brief summary. *Geological Society of America Memoirs* 206:1-19 %@ 0072-1069.

Heckel, P. H., M. R. Gibling, and N. R. King. 1998. Stratigraphic model for glacial-eustatic Pennsylvanian cyclothems in highstand nearshore detrital regimes. *The Journal of Geology* 106 (4):373-384.

Humphris, S. E. 1984. The mobility of the rare earth elements in the crust. *Rare earth element geochemistry* 2:317-342.

Ingri, J., A. Widerlund, M. Land, Ö. Gustafsson, P. Andersson, and B. Öhlander. 2000. Temporal variations in the fractionation of the rare earth elements in a boreal river; the role of colloidal particles. *Chemical Geology* 166 (1):23-45.

Jennings, S. R., P. S. Blicker, and D. R. Neuman. 2008. *Acid mine drainage and effects on fish health and ecology: a review*: Reclamation Research Group.

Johannesson, K. H., and X. Zhou. 1999. Origin of middle rare earth element enrichments in acid waters of a Canadian High Arctic lake. *Geochimica et Cosmochimica Acta* 63 (1):153-165.

Johnson, D. B., and K. B. Hallberg. 2005. Acid mine drainage remediation options: a review. *Sci Total Environ* 338 (1-2):3-14.

Joosu, L., A. Lepland, T. Kreitsmann, K. Üpraus, N. M. W. Roberts, P. Paiste, A. P. Martin, and K. Kirsimäe. 2016. Petrography and the REE-composition of apatite in the Paleoproterozoic Pilgujärvi Sedimentary Formation, Pechenga Greenstone Belt, Russia. *Geochimica et Cosmochimica Acta* 186 (Supplement C):135-153.

Karacan, C. Ö. 2009. Reservoir rock properties of coal measure strata of the Lower Monongahela Group, Greene County (Southwestern Pennsylvania), from methane control and production perspectives. *International Journal of Coal Geology* 78 (1):47-64.

Klein, G. D., and J. B. Kupperman. 1992. Pennsylvanian cyclothems: Methods of distinguishing tectonically induced changes in sea level from climatically induced changes. *Geological Society of America Bulletin* 104 (2):166-175.

Leybourne, M. I., and B. L. Cousens. 2005. Rare earth elements (REE) and Nd and Sr isotopes in groundwater and suspended sediments from the Bathurst Mining Camp, New Brunswick: water-rock reactions and elemental fractionation. *Rare Earth Elements in Groundwater Flow Systems*:253-293.

Leybourne, M. I., W. D. Goodfellow, D. R. Boyle, and G. M. Hall. 2000. Rapid development of negative Ce anomalies in surface waters and contrasting REE patterns in groundwaters associated with Zn–Pb massive sulphide deposits. *Applied Geochemistry* 15 (6):695-723.

McLennan, S., S. Hemming, D. McDaniel, and G. Hanson. 1993. Geochemical approaches to sedimentation, provenance, and tectonics. *Geological Society of America Special Papers* 284:21-40.

Merten, D., and G. Buchel. 2004. Determination of Rare Earth Elements in Acid Mine Drainage by Inductively Coupled Plasma Mass Spectrometry. *Microchimica Acta* 148 (3-4):163-170.

Merten, D., J. Geletneky, H. Bergmann, G. Haferburg, E. Kothe, and G. Büchel. 2005. Rare earth element patterns: A tool for understanding processes in remediation of acid mine drainage. *Chemie der Erde - Geochemistry* 65:97-114.

Nagasawa, H. 1970. Rare earth concentrations in zircons and apatites and their host dacites and granites. *Earth and Planetary Science Letters* 9 (4):359-364.

Nordstrom, D., and C. Alpers. 1999. *Geochemistry of acid mine waters*.

Nordstrom, D. K. 2011. Hydrogeochemical processes governing the origin, transport and fate of major and trace elements from mine wastes and mineralized rock to surface waters. *Applied Geochemistry* 26 (11):1777-1791.

Nordstrom, D. K., D. W. Blowes, and C. J. Ptacek. 2015. Hydrogeochemistry and microbiology of mine drainage: An update. *Applied Geochemistry* 57:3-16.

Olías, M., J. Cerón, I. Fernández, and J. De la Rosa. 2005. Distribution of rare earth elements in an alluvial aquifer affected by acid mine drainage: the Guadiamar aquifer (SW Spain). *Environmental Pollution* 135 (1):53-64.

Patchett, P. J., G. M. Ross, and J. D. Gleason. 1999. Continental drainage in North America during the Phanerozoic from Nd isotopes. *Science* 283 (5402):671-673

Pérez-López, R., J. Delgado, J. M. Nieto, and B. Márquez-García. 2010. Rare earth element geochemistry of sulphide weathering in the São Domingos mine area (Iberian Pyrite Belt): A proxy for fluid–rock interaction and ancient mining pollution. *Chemical Geology* 276 (1-2):29-40.

Phan, T. T., J. B. Gardiner, R. C. Capo, and B. W. Stewart. 2017. Geochemical and multi-isotopic (87Sr/86Sr, 143Nd/144Nd, 238U/235U) perspectives of sediment sources, depositional conditions, and diagenesis of the Marcellus Shale, Appalachian Basin, USA. . *Geochimica et Cosmochimica Acta*.

Plumlee, G., K. Smith, M. Montour, W. Ficklin, and E. Mosier. 1999. Geologic controls on the composition of natural waters and mine waters draining diverse mineral-deposit types.

The environmental geochemistry of mineral deposits, Reviews in Economic Geology 6:373-432.

Ruppert, L. 2000. US Geological Survey Professional Paper, 1625-C, Chapter A–Executive Summary–Coal Resource Assessment of Selected Coal Beds and Zones in the Northern and Central Appalachian Basin Coal Regions. *DC: US Geological Survey Professional Paper*

A1-A3.

Ruppert, L. F., M. A. Kirschbaum, P. D. Warwick, R. M. Flores, R. H. Affolter, and J. R. Hatch. 2002. The US Geological Survey's national coal resource assessment: the results. *International Journal of Coal Geology* 50 (1):247-274.

Ruppert, L. F., and C. L. Rice. 2000. US Geological Survey Professional Paper, 1625-C, Chapter B - Coal Resource Assessment Methodology and Geology of the Northern and Central Appalachian Basin Coal Regions. *DC: US Geological Survey Professional Paper*:B8.

Ruppert, L. F., S. J. Tewalt, L. J. Bragg, and R. N. Wallack. 1999. A digital resource model of the Upper Pennsylvanian Pittsburgh coal bed, Monongahela Group, northern Appalachian basin coal region, USA. *International Journal of Coal Geology* 41 (1):3-24.

Schatzel, S. J., and B. W. Stewart. 2012. A provenance study of mineral matter in coal from Appalachian Basin coal mining regions and implications regarding the respirable health of underground coal workers: A geochemical and Nd isotope investigation. *International Journal of Coal Geology* 94:123-136.

Seredin, V., and I. Y. Chekryzhov. 2011. Ore potentiality of the Vanchin Graben, Primorye, Russia. *Geology of Ore Deposits* 53 (3):202-220.

Seredin, V. V., and S. Dai. 2012. Coal deposits as potential alternative sources for lanthanides and yttrium. *International Journal of Coal Geology* 94:67-93.

Serrano, M. J. G., L. F. A. Sanz, and D. K. Nordstrom. 2000. REE speciation in low-temperature acidic waters and the competitive effects of aluminum. *Chemical Geology* 165 (3):167-180.

Sholkovitz, E. R. 1995. The aquatic chemistry of rare earth elements in rivers and estuaries. *Aquatic Geochemistry* 1 (1):1-34.

Simate, G. S., and S. Ndlovu. 2014. Acid mine drainage: Challenges and opportunities. *Journal of Environmental Chemical Engineering* 2 (3):1785-1803.

Stewart, B. W., R. C. Capo, B. C. Hedin, and R. S. Hedin. 2017. Rare earth element resources in coal mine drainage and treatment precipitates in the Appalachian Basin, USA. *International Journal of Coal Geology* 169:28-39.

Sun, H., F. Zhao, M. Zhang, and J. Li. 2012. Behavior of rare earth elements in acid coal mine drainage in Shanxi Province, China. *Environmental Earth Sciences* 67 (1):205-213.

Tang, J., and K. H. Johannesson. 2003. Speciation of rare earth elements in natural terrestrial waters: assessing the role of dissolved organic matter from the modeling approach. *Geochimica et Cosmochimica Acta* 67 (13):2321-2339.

Tewalt, S., L. Ruppert, R. Carlton, D. Bresinski, R. Wallack, and L. Bragg. 2001. A digital resource model for the Upper Pennsylvanian Pittsburgh coal bed, Monongahela Group, Northern Appalachian Basin Coal Region. *US Geological Survey Professional Paper*.

USGS, U. S. G. S. 2017. *Coal Mine Drainage Projects in Pennsylvania* U.S. Department of Interior 2010 [cited 2017]. Available from https://pa.water.usgs.gov/projects/energy/amd/.

Verplanck, P. L. 2013. Partitioning of Rare Earth Elements between Dissolved and Colloidal Phases. *Procedia Earth and Planetary Science* 7:867-870.

Verplanck, P. L., D. K. Nordstrom, and H. E. Taylor. 1999. Overview of rare earth element investigations in acid waters of US Geological Survey abandoned mine lands watersheds. *US Geol. Surv. Wat. Resourc. Invest. Rep*:83-92.

Verplanck, P. L., D. K. Nordstrom, H. E. Taylor, and B. A. Kimball. 2004. Rare earth element partitioning between hydrous ferric oxides and acid mine water during iron oxidation. *Applied Geochemistry* 19 (8):1339-1354.

Viers, J., B. Dupré, M. Polvé, J. Schott, J.-L. Dandurand, and J.-J. Braun. 1997. Chemical weathering in the drainage basin of a tropical watershed (Nsimi-Zoetele site, Cameroon): comparison between organic-poor and organic-rich waters. *Chemical Geology* 140 (3-4):181-206.

Watson, W. D., L. F. Ruppert, S. J. Tewalt, and L. J. Bragg. 2001. The Upper Pennsylvanian Pittsburgh coal bed: resources and mine models. *Natural Resources Research* 10 (1):21-34.

Welch, S. A., A. G. Christy, L. Isaacson, and D. Kirste. 2009. Mineralogical control of rare earth elements in acid sulfate soils. *Geochimica et Cosmochimica Acta* 73 (1):44-64.

Winters, W. R., and R. C. Capo. 2004. Ground water flow parameterization of an Appalachian coal mine complex. *Ground water* 42 (5):700-710.

Wood, S. A., W. M. Shannon, and L. Baker. 2005. The Aqueous Geochemistry of the Rare Earth Elements and Yttrium. Part 13: REE Geochemistry of Mine Drainage from the Pine Creek Area, Coeur d'Alene River Valley, Idaho, USA, 89-110. Dordrecht: Springer Netherlands.

Worrall, F., and D. Pearson. 2001. The development of acidic groundwaters in coal-bearing strata: Part I. Rare earth element fingerprinting. *Applied Geochemistry* 16 (13):1465-1480.

Xu, Z., and G. Han. 2009. Rare earth elements (REE) of dissolved and suspended loads in the Xijiang River, South China. *Applied Geochemistry* 24 (9):1803-1816.

Younger, P. 1997. The longevity of minewater pollution: a basis for decision-making. *Science of the Total Environment* 194:457-466.

Zhao, F., Z. Cong, H. Sun, and D. Ren. 2007. The geochemistry of rare earth elements (REE) in acid mine drainage from the Sitai coal mine, Shanxi Province, North China. *International Journal of Coal Geology* 70 (1-3):184-192.

Ziemkiewicz, P., T. He, A. Noble, and X. Liu. 2016. Recovery of Rare Earth Elements (REEs) from Coal Mine Drainage. In *2016 Mine Drainage Task Force Symposium*. Waterfront Place Hotel, Morgantown, West Virginia: West Virginia Mine Drainage Task Force.